

Pontryagin-Guided Deep Learning for Large-Scale Constrained Dynamic Portfolio Choice

Jeonggyu Huh¹, Hyeng Keun Koo², and Jaegi Jeon^{*3}

¹Department of Mathematics, Sungkyunkwan University, Republic of Korea

²Department of Financial Engineering, Ajou University, Republic of Korea

³Graduate School of Data Science, Chonnam National University, Republic of Korea

January 31, 2025

Abstract

We present a Pontryagin-Guided Direct Policy Optimization (**PG-DPO**) method for *constrained* dynamic portfolio choice—incorporating consumption and multi-asset investment—that scales to *thousands* of risky assets. By combining neural-network controls with Pontryagin’s Maximum Principle (PMP), it circumvents the curse of dimensionality that renders dynamic programming (DP) grids intractable beyond a handful of assets. Unlike value-based PDE or BSDE approaches, PG-DPO enforces PMP conditions at each gradient step, naturally accommodating no-short-selling or borrowing constraints and optional consumption bounds. A “one-shot” variant rapidly computes Pontryagin-optimal controls after a brief warm-up, leading to substantially higher accuracy than naive baselines. On modern GPUs, near-optimal solutions typically arise in around ten minutes, and refining to higher precision usually takes under an hour. Numerical experiments show that in the unconstrained case, PG-DPO recovers the known closed-form solution even at 10,000 assets, while under constraints it remains tractable up to 1,000 assets—both well beyond the long-standing DP-based limit of fewer than seven.

1 Introduction

Dynamic portfolio choice—how an investor should optimally allocate wealth among multiple assets and consume over time under uncertainty—is a cornerstone of

*Corresponding Author: jaegijeon@jnu.ac.kr

modern finance. Classic studies by Samuelson (1975) and Merton (1969, 1971) pioneered both continuous-time and discrete-time frameworks in which investors balance growth, risk, and consumption. Under certain idealized assumptions (e.g., complete markets, unlimited short-selling/borrowing, and frictionless trade), this “Merton problem” admits elegant (semi-)closed-form solutions (e.g., Kim & Omberg, 1996; Liu, 2007). However, real-world markets exhibit numerous *constraints*—such as short-sale bans, borrowing limits, minimum consumption requirements, or ratcheting rules that prevent consumption from dropping below past peaks—which invalidate the unconstrained, frictionless assumption. These practical features significantly complicate the analysis and typically necessitate more flexible numerical or simulation-based techniques.

Over the last several decades, a rich literature has emerged that generalizes the Merton framework to incorporate *policy constraints*. For instance, prohibitions on short sales or leverage can be encoded through nonnegative constraints on asset holdings, leading to boundary conditions in the Hamilton–Jacobi–Bellman (HJB) equation or to variational inequalities in cases where the optimal policy “touches” the boundary (e.g., Karatzas et al., 1987; Cvitanic & Karatzas, 1996). Borrowing constraints similarly restrict leverage and can require explicit state-space truncation (Karatzas & Shreve, 1998). On the consumption side, real-life policies or economic frictions may impose either lower bounds (to cover essential expenses) or upper limits, leading to quasi-variational inequalities when multiple constraints interact (Shreve & Soner, 1994; Fleming & Soner, 2006). Additionally, *consumption ratcheting* (Dybvig, 1995) disallows consumption from falling below a previously attained level, capturing behavioral or habit-formation effects (Constantinides, 1990; Sundaresan, 1989). In all these situations, the classical closed-form Merton solution ceases to apply, and one must resort to more general numerical schemes.

Even without constraints, dynamic programming (DP) methods for multi-asset Merton problems tend to suffer from the curse of dimensionality as the number of assets grows. For example, Campbell & Viceira (1999, 2001); Campbell et al. (2003) incorporate multiple state variables (such as dividend yields and interest rates) but limit the number of risky assets to fewer than seven for tractability. Empirical studies by Balduzzi & Lynch (1999), Lynch & Balduzzi (2000); Lynch (2001), and Brandt et al. (2005) add learning or transaction costs, yet still consider only small portfolios. More advanced techniques (Buraschi et al., 2010; Garlappi & Skoulakis, 2010; Jurek & Viceira, 2011) cannot fully evade the exponential blow-up in high-dimensional DP grids. Introducing constraints (e.g., short-selling bans, consumption floors) on top of many risky assets further amplifies computational complexity. Consequently, constrained Merton problems in moderate or large dimensions remain a significant challenge, pushing researchers to explore alternative approaches.

In this work, we develop a scalable framework that accommodates *thousands* of assets while naturally handling constraints such as no short-selling or borrowing. Building on Pontryagin’s Maximum Principle (PMP), we propose a *policy-centric* approach—rather than the usual value-based method—to directly learn optimal controls via neural networks (Sections 3–4). Our method avoids intractable DP grids and instead uses stochastic-gradient updates guided by the Pontryagin adjoint (costate) processes. The result is a *Pontryagin-Guided Direct Policy Optimization (PG-DPO)* algorithm that can flexibly incorporate log-barrier or KKT-based mechanisms to enforce short-sale or borrowing constraints, as well as possible upper/lower consumption bounds.

Moreover, we develop a *PG-DPO-OneShot* variant that uses a brief network warm-up, then *directly* computes the Pontryagin-optimal controls (e.g., via a small-scale Newton solve under log-barriers) at each time–state, bypassing further network inference while still respecting all constraints. This approach often yields accuracy improvements compared to naive baselines and remains tractable even at extreme scales (e.g., thousands of assets on a single GPU).

Recent years have seen growing interest in deep learning methods for continuous-time stochastic control, including deep BSDE techniques (Han et al., 2018; Weinan, 2017), physics-informed neural networks (Raissi et al., 2019), and reinforcement learning (Dai et al., 2023). However, most of these approaches rely on approximating *value functions* or PDE solutions, which become prohibitively difficult to handle with large state/action spaces or with intricate constraints like short-sale bans and consumption ratcheting. By contrast, our direct policy optimization method circumvents the explicit value-function approximation, facilitating scalability to tens of thousands of assets and straightforward enforcement of portfolios and consumption constraints. Indeed, the policy merely outputs feasible controls (e.g., via softmax or barrier-based projection), while the Pontryagin adjoint ensures that gradient updates align with optimality conditions in a forward–backward SDE sense.

Our contributions can be summarized as follows:

1. We formulate a large-scale, continuous-time portfolio–consumption problem under realistic constraints (e.g., no short-selling or borrowing, optional consumption bounds), highlighting how the classical Merton approach breaks down in such scenarios (Section 2).
2. We develop the **PG-DPO** framework, which parameterizes both investment and consumption controls via neural networks, and show how *Pontryagin’s Maximum Principle* can guide the training even in the presence of constraints (Section 3).

3. We propose a **PG-DPO-OneShot** scheme that leverages a brief warm-up to stabilize the Pontryagin adjoint, then computes closed-form or barrier-based solutions for the constrained controls at each time step, boosting accuracy and scalability (Section 4).
4. Through numerical experiments (Section 5), we demonstrate that our approach scales to thousands of assets, delivers near-optimal solutions, and enforces constraints effectively without resorting to high-dimensional PDE grids.

We conclude in Section 6 with a discussion of potential extensions, such as integrating transaction costs, consumption ratcheting, or robust control ideas. Overall, this work shows that truly large-scale, *constrained* dynamic portfolio choice in a continuous-time setting—an enduring challenge in mathematical finance—can be made tractable with Pontryagin-guided, neural-network-based approaches.

2 Multi-Asset Continuous-Time Portfolio Problem

In this section, we present a multi-asset version of Merton’s classic portfolio problem (Merton, 1971), wherein an investor allocates wealth among multiple risky assets and a risk-free asset while also consuming continuously. Unlike the single-asset case, the presence of multiple (potentially correlated) assets with distinct drifts and volatilities leads to richer portfolio strategies and more challenging solution methods. In particular, although the *wealth* itself remains one-dimensional, the *investment decision* can span multiple dimensions, reflecting the investor’s choices across different risky assets.

2.1 Problem Formulation and Neural Network Parametrization of Controls

We consider $n + 1$ assets, indexed by $i = 0, 1, \dots, n$. The 0th asset is risk-free with drift r_t and zero volatility, while the remaining n assets are risky with drifts $\mu_{i,t}$ for $i = 1, \dots, n$ and covariance $\Sigma_t \in \mathbb{R}^{n \times n}$. The n -dimensional drift vector for the risky assets is defined as $\boldsymbol{\mu}_t = (\mu_{1,t}, \dots, \mu_{n,t})^\top \in \mathbb{R}^n$. By setting $\mu_{0,t} := r_t$ as the drift of the risk-free asset, the $(n + 1)$ -dimensional vector encompassing all assets’ drifts is given by $\tilde{\boldsymbol{\mu}}_t = (r_t, \mu_{1,t}, \dots, \mu_{n,t})^\top \in \mathbb{R}^{n+1}$.

Next, we define a matrix $\tilde{V}_t \in \mathbb{R}^{(n+1) \times n}$ such that its 0th row is all zeros, reflecting the zero volatility of the risk-free asset, and the submatrix V_t governs the n risky assets. Specifically, $\tilde{V}_{t,0,*} = \mathbf{0}$ and $\tilde{V}_{t,1:n,*} = V_t$, where $\Sigma_t = V_t V_t^\top$.

Let X_t denote the total wealth, and let $\boldsymbol{\pi}_t = (\pi_{0,t}, \pi_{1,t}, \dots, \pi_{n,t})^\top$ represent the portfolio weights satisfying $\sum_{i=0}^n \pi_{i,t} = 1$. Here, $\pi_{0,t}$ is the fraction invested in the risk-free asset, and $\pi_{i,t}$ for $i \geq 1$ is the fraction invested in the i th risky asset. The investor's consumption rate C_t is nonnegative, i.e., $C_t \geq 0$. The wealth X_t evolves according to the stochastic differential equation (SDE):

$$dX_t = \left(X_t \boldsymbol{\pi}_t^\top \tilde{\boldsymbol{\mu}}_t - C_t \right) dt + X_t \boldsymbol{\pi}_t^\top \tilde{V}_t d\mathbf{W}_t, \quad X_0 = x_0 > 0, \quad (1)$$

where $\mathbf{W}_t \in \mathbb{R}^n$ is an n -dimensional standard Brownian motion. Note that $\tilde{\boldsymbol{\mu}}_{t,0} = r_t$ and $\tilde{V}_{t,0,*} = \mathbf{0}$, ensuring that the risk-free component has drift r_t with no stochastic part.

The utility maximization objective is formulated in continuous time, analogous to the classical Merton problem:

$$J(\boldsymbol{\pi}_t, C_t) = \mathbb{E} \left[\int_0^T e^{-\rho t} U(C_t) dt + \kappa e^{-\rho T} U(X_T) \right], \quad (2)$$

where $\rho > 0$ is a continuous discount rate, $\kappa > 0$ is a bequest parameter, and U is a CRRA utility function defined as:

$$U(x) = \begin{cases} \frac{x^{1-\gamma}}{1-\gamma}, & \gamma > 0, \gamma \neq 1, \\ \ln(x), & \gamma = 1, \end{cases} \quad (3)$$

where γ represents the investor's relative risk aversion: higher $\gamma > 1$ corresponds to greater risk aversion, while $\gamma < 1$ indicates lower aversion. The logarithmic case ($\gamma = 1$) is recovered continuously as $\gamma \rightarrow 1$.

To solve this high-dimensional control problem, the controls are typically parameterized using neural networks:

$$\boldsymbol{\pi}_t = \boldsymbol{\pi}_\theta(t, X_t) \in \mathbb{R}^n, \quad C_t = C_\phi(t, X_t), \quad (4)$$

where θ and ϕ denote the neural network parameters. The training objective is then $J(\theta, \phi) \approx J(\boldsymbol{\pi}_t, C_t)$, and numerical methods are applied to identify a locally or globally optimal policy.

2.2 Constraints on Portfolio Choice and Consumption

In many real-world portfolio settings, investors face constraints that limit the admissible set of controls $(\boldsymbol{\pi}_t, C_t)$. Below, we outline two main classes of constraints: nonnegative portfolio weights, which encompass no short-selling and no borrowing, and bounds on consumption.

First, we consider nonnegative portfolio weights. Each weight $\pi_{i,t}$ is required to satisfy

$$\pi_{i,t} \geq 0 \quad \text{for } i = 0, 1, \dots, n.$$

Here, $\pi_{0,t}$ represents the fraction of wealth in the risk-free asset, and $\pi_{i,t}$ for $i = 1, \dots, n$ are the fractions in risky assets. Because these fractions must be nonnegative, we naturally exclude both short-selling, which would require $\pi_{i,t} < 0$ for some risky asset i , and borrowing beyond wealth, i.e., a negative position in the risk-free asset ($\pi_{0,t} < 0$) to leverage the risky assets. Combined with the full-investment condition $\sum_{i=0}^n \pi_{i,t} = 1$, these nonnegativity constraints ensure a simple, long-only portfolio with no leverage.

Second, consumption rates can also be subject to practical or regulatory requirements. For example, the consumption rate C_t must satisfy

$$C_{\min} \leq C_t \leq C_{\max},$$

where $C_{\min} > 0$ might capture mandatory living expenses, and $C_{\max} < \infty$ might limit overconsumption. More generally, one could allow C_{\min} or C_{\max} to be functions of time, such as to reflect seasonal patterns, or of the market path $S_{<t}$, such as adaptively tightening consumption bounds during downturns.

Beyond nonnegative weights and consumption bounds, many other constraints and market frictions can be incorporated. These include transaction costs or liquidity limits, which effectively modify the wealth dynamics to penalize excessive rebalancing, and taxes or regulatory constraints, such as maximum capital-gain distributions. While these issues are not our primary focus, the Pontryagin-based framework (Sections 3 and 4) could, in principle, be extended to such settings by restricting the control set or adjusting the state equations. However, such extensions may require methodological adjustments, which lie outside the scope of this paper.

In summary, we focus on a scenario where nonnegative portfolio weights $\pi_{i,t} \geq 0$ and a full-investment constraint $\sum_{i=0}^n \pi_{i,t} = 1$ jointly preclude both short-selling and borrowing. In the following sections, we demonstrate how our framework can handle these constraints numerically even when the number of assets is large. While we primarily focus on nonnegative portfolio weights, the consumption constraints can be addressed using similar techniques. Furthermore, if one wishes to allow leverage or certain short positions, it suffices to relax these bounds, such as $\pi_{0,t} \geq -\alpha$ or $\pi_{i,t} \geq -\beta$ for some $\alpha, \beta > 0$, or incorporate more general time-varying limits $[a_i(t), b_i(t)]$. The same methodology applies, under suitable modifications to the admissible set \mathcal{A} .

2.3 Closed-Form Solutions without Constraints

In some simplified versions of the finite-horizon Merton problem—specifically, unconstrained portfolio choice (no short-sale or leverage limits), CRRA utility, and deterministic parameters $\boldsymbol{\mu}_t, \Sigma_t, r_t$ (allowing either constant or explicit time dependence)—it is possible to derive closed-form solutions for the portfolio strategy and consumption rate. Below, we outline the core result, keeping in mind that any additional constraints typically invalidate such a closed-form derivation.

If there are no constraints on $\boldsymbol{\pi}_{1:n,t}$ aside from full investment $\pi_{0,t} + \sum_{i=1}^n \pi_{i,t} = 1$, and $(\boldsymbol{\mu}_t, \Sigma_t, r_t)$ are deterministic in t , one can often solve the associated HJB equation to obtain a time-invariant (or explicitly time-dependent) investment proportion:

$$\boldsymbol{\pi}_{1:n,t}^* = \frac{1}{\gamma} \Sigma_t^{-1} (\boldsymbol{\mu}_t - r_t \mathbf{1}), \quad \pi_{0,t}^* = 1 - \sum_{i=1}^n \pi_{i,t}^*.$$

In the simplest case where $\boldsymbol{\mu}_t, \Sigma_t, r_t$ are truly constant (i.e., $\boldsymbol{\mu}, \Sigma, r$ do not vary with t), the above fraction $\boldsymbol{\pi}_{1:n,t}^*$ is indeed constant in time. If, however, $\boldsymbol{\mu}_t, \Sigma_t, r_t$ vary deterministically with t , the HJB solution may induce an explicit time dependence in $\boldsymbol{\pi}_{1:n,t}^*$. Nevertheless, closed-form or semi-analytic formulas are still available in many cases for specific functional forms of $\boldsymbol{\mu}_t$ and Σ_t .

By contrast, the optimal consumption rate C_t^* in a finite horizon $[0, T]$ generally takes the form

$$C_t^* = \alpha(t) X_t,$$

where $\alpha(t)$ is a time-dependent function determined via a backward solution of the HJB equation. For instance, if $\boldsymbol{\mu}_t, \Sigma_t, r_t$ are all constant in t , a well-known closed-form result is

$$\alpha(t) = \frac{\kappa}{\gamma} (1 - e^{-\kappa(T-t)})^{-1},$$

where the decay rate κ is given by

$$\kappa = \rho - (1 - \gamma) \left(r + \frac{(\boldsymbol{\mu} - r\mathbf{1})^\top \Sigma^{-1} (\boldsymbol{\mu} - r\mathbf{1})}{2\gamma} \right).$$

Hence, the consumption fraction $\alpha(t)$ explicitly depends on the remaining horizon $T - t$, decaying exponentially as $t \rightarrow T$.

Crucially, these closed-form expressions assume there are no constraints such as short-sale or leverage limits, margin requirements, or path-dependent restrictions. In practice, once even a basic constraint is introduced, the HJB-based analytical solution typically breaks down, necessitating numerical methods. Our proposed Pontryagin-Guided Direct Policy Optimization (Section 4) is one such scalable approach, capable of handling high-dimensional or constraint-rich problems beyond the reach of closed-form Merton formulas.

3 Pontryagin's Principle for Multi-Asset Portfolio Problem

We now discuss how Pontryagin's Maximum Principle (PMP) applies to the *multi-asset, continuous-time* Merton problem introduced in Section 2.1. Although the *wealth* X_t itself is a single-dimensional state, the presence of multiple risky assets can introduce higher-dimensional controls $\boldsymbol{\pi}_t \in \mathbb{R}^n$.

In particular, we first derive the adjoint (costate) processes for the unconstrained case, where no restrictions are imposed on the portfolio weights $\boldsymbol{\pi}_t$. We then extend this analysis to the constrained case, where nonnegative portfolio weights $\pi_{i,t} \geq 0$ and the full-investment condition $\sum_{i=0}^n \pi_{i,t} = 1$ are enforced, as discussed in Section 2.2. In both scenarios, we explore the relationship between the adjoint processes and the optimal policies, as well as their implications for suboptimal (parameterized) policies in this multi-asset setting.

3.1 Pontryagin's Maximum Principle for the Continuous-Time Portfolio Problem

We now apply Pontryagin's Maximum Principle to the continuous-time portfolio model outlined in Section 2.1. See Pontryagin, 2018; Pardoux & Peng, 1990; Fleming & Soner, 2006; Pham, 2009 for further details on PMP. Following Pontryagin's Maximum Principle, we introduce a scalar adjoint $\lambda_t \approx \frac{\partial J}{\partial X_t}$, tied to the state X_t in the utility maximization objective J defined in (2), and a vector adjoint $\mathbf{Z}_t \in \mathbb{R}^n$, tied to the n -dimensional Brownian motion \mathbf{W}_t .

The Hamiltonian then takes the form

$$\mathcal{H}(t, X_t, \boldsymbol{\pi}_t, C_t, \lambda_t, \mathbf{Z}_t) = e^{-\rho t} U(C_t) + \lambda_t \left[X_t \boldsymbol{\pi}_t^\top \tilde{\boldsymbol{\mu}}_t - C_t \right] + \mathbf{Z}_t^\top (X_t \tilde{\mathbf{V}}_t^\top \boldsymbol{\pi}_t), \quad (5)$$

where λ_t captures the marginal value of X_t , and \mathbf{Z}_t captures sensitivities to the Brownian shocks \mathbf{W}_t .

When the controls $(\boldsymbol{\pi}_t^*, C_t^*)$ are optimal, the wealth process X_t^* and adjoint processes $(\lambda_t^*, \mathbf{Z}_t^*)$ jointly satisfy the *coupled forward-backward Pontryagin system*:

$$\begin{aligned} dX_t^* &= \left[X_t^* (\boldsymbol{\pi}_t^*)^\top \tilde{\boldsymbol{\mu}}_t - C_t^* \right] dt + X_t^* (\boldsymbol{\pi}_t^*)^\top \tilde{\mathbf{V}}_t d\mathbf{W}_t, \quad X_0^* = x_0 > 0, \quad (6) \\ d\lambda_t^* &= -\frac{\partial \mathcal{H}}{\partial X} \left(t, X_t^*, \boldsymbol{\pi}_t^*, C_t^*, \lambda_t^*, \mathbf{Z}_t^* \right) dt + \mathbf{Z}_t^{*\top} d\mathbf{W}_t, \quad \lambda_T^* = \frac{\partial}{\partial X} \left[\kappa e^{-\rho T} U(X_T^*) \right]. \end{aligned}$$

Here, X_t^* follows the same structural dynamics as (1) but with optimal controls $\boldsymbol{\pi}_t^*$ and C_t^* , while λ_t^* and \mathbf{Z}_t^* solve the backward adjoint equation. The coupling arises because $\boldsymbol{\pi}_t^*$ and C_t^* depend on λ_t^* , which in turn depends on X_t^* through $\partial \mathcal{H} / \partial X$.

This closed-loop structure distinguishes optimal trajectories from generic solutions to (1).

Additionally, at each t , $(\boldsymbol{\pi}_t^*, C_t^*)$ maximizes the Hamiltonian \mathcal{H} locally, yielding the first-order conditions

$$\frac{\partial \mathcal{H}}{\partial C_t} = e^{-\rho t} U'(C_t^*) - \lambda_t^* = 0, \quad \frac{\partial \mathcal{H}}{\partial \boldsymbol{\pi}_t} = \lambda_t^* X_t^* \tilde{\boldsymbol{\mu}}_t + X_t^* \tilde{\mathbf{V}}_t^\top \mathbf{Z}_t^* = \mathbf{0}.$$

Hence, one obtains

$$e^{-\rho t} U'(C_t^*) = \lambda_t^*, \quad \tilde{\mathbf{V}}_t^\top \mathbf{Z}_t^* = -\lambda_t^* \tilde{\boldsymbol{\mu}}_t.$$

Given the utility function U in (3), its marginal is $U'(c) = c^{-\gamma}$. Substituting into $e^{-\rho t} U'(C_t^*) = \lambda_t^*$ directly yields:

$$C_t^* = \left(e^{\rho t} \lambda_t^* \right)^{-\frac{1}{\gamma}}. \quad (7)$$

Thus, the optimal consumption rate depends on λ_t^* but does not explicitly require its full functional form, thanks to the power-law structure.

A common result from the backward SDE for λ_t^* (or by differentiating \mathcal{H} w.r.t. X_t) is

$$\mathbf{Z}_t^* = (\partial_x \lambda_t^*) \left(X_t^* \tilde{\mathbf{V}}_t^\top \boldsymbol{\pi}_t^* \right), \quad (8)$$

which says that \mathbf{Z}_t^* equals the product of $(X_t^* \tilde{\mathbf{V}}_t^\top \boldsymbol{\pi}_t^*)$ and the scalar $\partial_x \lambda_t^*$. For the sub-vector $\mathbf{Z}_{1:n,t}^* \in \mathbb{R}^n$ of \mathbf{Z}_t^* (the part tied to the n risky Brownian directions), one often has

$$\mathbf{V}_t^\top \mathbf{Z}_{1:n,t}^* = -\lambda_t^* (\mu_{1,t} - r_t, \dots, \mu_{n,t} - r_t)^\top,$$

while from

$$\mathbf{Z}_{1:n,t}^* = (\partial_x \lambda_t^*) X_t^* \mathbf{V}_t^\top (\boldsymbol{\pi}_{1:n,t}^*),$$

one obtains

$$\mathbf{V}_t^\top \left[(\partial_x \lambda_t^*) X_t^* \mathbf{V}_t^\top \boldsymbol{\pi}_{1:n,t}^* \right] = -\lambda_t^* (\mu_{1,t} - r_t, \dots, \mu_{n,t} - r_t)^\top.$$

Solving for $\boldsymbol{\pi}_{1:n,t}^*$ yields

$$\boldsymbol{\pi}_{1:n,t}^* = -\frac{\lambda_t^*}{X_t^* (\partial_x \lambda_t^*)} \Sigma_t^{-1} (\boldsymbol{\mu}_t - r_t \mathbf{1}), \quad (9)$$

recovering the familiar $\Sigma_t^{-1} (\boldsymbol{\mu}_t - r_t \mathbf{1})$ shape in multi-asset Merton problems.

Overall, Pontryagin's approach reduces the continuous-time control problem to a forward-backward SDE (for $X_t^*, \lambda_t^*, \mathbf{Z}_t^*$) plus a pointwise maximization yielding closed-form formulas for $(\boldsymbol{\pi}_t^*, C_t^*)$. In modern ML frameworks (e.g., PyTorch), one can compute these adjoints automatically by backpropagating through stochastic rollouts of X_t , thus avoiding PDE or grid-based methods. This principle underlies the neural Pontryagin-based algorithms introduced later.

3.2 Extending Pontryagin's Maximum Principle to Constrained Portfolio Problems

3.2.1 KKT-Based Approach to Constrained Portfolio Problems

Many realistic portfolio settings impose constraints on the portfolio weights $\boldsymbol{\pi}_t$ or on consumption C_t . In this subsection, we illustrate how to incorporate such constraints using a KKT (Karush–Kuhn–Tucker) formulation (see Karush, 1939; Kuhn & Tucker, 2013, for foundational references) and further discussion in standard texts (e.g. Nocedal & Wright, 1999). We focus on the case $\pi_{i,t} \geq 0$ (i.e., no short-selling or borrowing) together with $\sum_{i=0}^n \pi_{i,t} = 1$, which signifies full investment in the risk-free plus n risky assets. Here, $\pi_{0,t}$ represents the proportion in the risk-free asset, while $\pi_{i,t}$ for $i \geq 1$ are the weights in the risky assets. Although we concentrate on these two constraints, the framework naturally extends to others discussed in Section 2.2.

We express these constraints via equality and inequality functions:

$$h(\boldsymbol{\pi}_t) = 1 - \sum_{i=0}^n \pi_{i,t} = 0, \quad g_i(\boldsymbol{\pi}_t) = -\pi_{i,t} \leq 0, \quad i = 0, \dots, n.$$

Next, we introduce the Lagrange multiplier η_t for the equality constraint and multipliers $\zeta_{i,t} \geq 0$ for the inequalities. We then build an augmented Hamiltonian:

$$\tilde{\mathcal{H}}_{\text{KKT}} = \mathcal{H} + \eta_t h(\boldsymbol{\pi}_t) + \sum_{i=0}^n \zeta_{i,t} g_i(\boldsymbol{\pi}_t), \quad (10)$$

where \mathcal{H} is the standard Pontryagin Hamiltonian $\mathcal{H}(t, X_t, \boldsymbol{\pi}_t, C_t, \boldsymbol{\lambda}_t, \mathbf{Z}_t)$. By KKT theory, the first-order optimality conditions at each time t become

$$\frac{\partial \tilde{\mathcal{H}}_{\text{KKT}}}{\partial \boldsymbol{\pi}_t} = \mathbf{0}, \quad h(\boldsymbol{\pi}_t) = 0, \quad g_i(\boldsymbol{\pi}_t) \leq 0, \quad \zeta_{i,t} \geq 0, \quad \zeta_{i,t} g_i(\boldsymbol{\pi}_t) = 0.$$

The partial derivative $\frac{\partial \tilde{\mathcal{H}}_{\text{KKT}}}{\partial \pi_{i,t}}$ incorporates both η_t and $\zeta_{i,t}$. Concretely,

$$\frac{\partial \tilde{\mathcal{H}}_{\text{KKT}}}{\partial \pi_{i,t}} = \frac{\partial \mathcal{H}}{\partial \pi_{i,t}} + \eta_t \frac{\partial h}{\partial \pi_{i,t}} + \zeta_{i,t} \frac{\partial g_i}{\partial \pi_{i,t}} = 0, \quad i = 0, \dots, n,$$

with $\frac{\partial h}{\partial \pi_{i,t}} = -1$ and $\frac{\partial g_i}{\partial \pi_{i,t}} = -1$ if $g_i = -\pi_{i,t}$. Since each $\zeta_{i,t} \geq 0$, we obtain a piecewise system:

$$\sum_{i=0}^n \pi_{i,t} = 1, \quad \zeta_{i,t} \pi_{i,t} = 0 \quad (\text{complementary slackness}).$$

Hence, if $\pi_{i,t} > 0$, then the multiplier $\zeta_{i,t}$ is zero (the inequality is inactive). Conversely, if $\pi_{i,t} = 0$, then $\zeta_{i,t} \geq 0$ may be strictly positive, enforcing the boundary.

If we *ignore* the constraints, the unconstrained Pontryagin solution for $\boldsymbol{\pi}_t$ might yield negative entries or fail to sum to one. The KKT system effectively *projects* this unconstrained solution onto the feasible simplex

$$\Delta^n = \left\{ \boldsymbol{\pi}_t \in \mathbb{R}^{n+1} \mid \sum_{i=0}^n \pi_{i,t} = 1, \pi_{i,t} \geq 0 \right\}.$$

Numerically, this often requires an iterative active-set method to determine which assets are pinned at zero and which remain positive while ensuring $\sum_{i=0}^n \pi_{i,t} = 1$. In short, the KKT conditions (cf. e.g. Karush, 1939; Kuhn & Tucker, 2013; Nocedal & Wright, 1999) act as a rigorous framework for enforcing no short-selling, no borrowing, and full investment within the Pontryagin approach.

3.2.2 Barrier-Based Approach to Constrained Portfolio Problems

The KKT approach provides a rigorous way to handle short-selling or borrowing constraints but becomes prohibitively expensive in high-dimensional settings due to the need to repeatedly solve large, piecewise nonlinear systems. An alternative is the *log-barrier* method (e.g., Fiacco & McCormick, 1990; Boyd, 2004; Nocedal & Wright, 1999), which enforces $\pi_{i,t} > 0$ by introducing a penalty term:

$$\Phi_\epsilon(\pi_{i,t}) = -\epsilon \ln(\pi_{i,t}), \quad \epsilon > 0.$$

As $\pi_{i,t} \rightarrow 0^+$, $\Phi_\epsilon(\pi_{i,t})$ diverges to $-\infty$, effectively preventing $\pi_{i,t}$ from approaching zero. This method ensures $\pi_{i,t} > 0$ smoothly and approximately, avoiding explicit boundary detection. As $\epsilon \rightarrow 0$, the solution converges to the unconstrained case, making the barrier approach practical for large-scale portfolio optimization.

To handle the constraints $\sum_{i=0}^n \pi_{i,t} = 1$ and $\pi_{i,t} > 0$, we augment the original Pontryagin Hamiltonian \mathcal{H} with a Lagrange multiplier η_t for the equality constraint and log-barrier terms $\Phi_\epsilon(\pi_{i,t})$ for the positivity constraints. The augmented Hamiltonian is given by:

$$\tilde{\mathcal{H}}_{\text{barrier}} = \mathcal{H} + \eta_t \left(1 - \sum_{i=0}^n \pi_{i,t} \right) + \epsilon \sum_{i=0}^n \ln(\pi_{i,t}). \quad (11)$$

Here, η_t enforces the sum-to-one constraint, while Φ_ϵ penalizes small $\pi_{i,t}$.

From the log-barrier terms, we derive the modified first-order conditions:

$$\frac{\partial \mathcal{H}}{\partial \pi_{i,t}} = \eta_t + \frac{\epsilon}{\pi_{i,t}}, \quad i = 0, \dots, n, \quad \text{with } \sum_{i=0}^n \pi_{i,t} = 1.$$

For instance, in a multi-asset Merton model with a risk-free asset $i = 0$ and n risky assets $i = 1, \dots, n$, we can write:

$$\frac{\partial \mathcal{H}}{\partial \pi_{0,t}} = \lambda_t^* X_t^* r_t = \eta_t + \frac{\epsilon}{\pi_{0,t}},$$

$$\frac{\partial \mathcal{H}}{\partial \pi_{i,t}} = \lambda_t^* X_t^* \mu_{i,t} + (\partial_x \lambda_t^*)(X_t^*)^2 [\Sigma_t \boldsymbol{\pi}_{t,1:n}^*]_i = \eta_t + \epsilon \frac{1}{\pi_{i,t}}, \quad i = 1, \dots, n.$$

Solving these simultaneously, together with $\sum_{i=0}^n \pi_{i,t} = 1$, yields a smooth approximation of the constrained optimum.

To implement the barrier method numerically, we define a function $\mathbf{F} : \mathbb{R}^{n+2} \rightarrow \mathbb{R}^{n+2}$ as:

$$\mathbf{F}(\boldsymbol{\pi}_t, \eta_t) = \left(F_0, \dots, F_n, F_{\text{sum}} \right)^\top,$$

where each component encodes either a barrier-FOC or the sum-to-one constraint:

$$F_i(\boldsymbol{\pi}_t, \eta_t) = \frac{\partial \mathcal{H}}{\partial \pi_{i,t}}(\boldsymbol{\pi}_t) - \left(\eta_t + \frac{\epsilon}{\pi_{i,t}} \right), \quad i = 0, \dots, n,$$

$$F_{\text{sum}}(\boldsymbol{\pi}_t, \eta_t) = \sum_{i=0}^n \pi_{i,t} - 1.$$

Finding $\mathbf{F}(\boldsymbol{\pi}_t, \eta_t) = \mathbf{0}$ is equivalent to solving:

$$\begin{cases} \frac{\partial \mathcal{H}}{\partial \pi_{i,t}}(\boldsymbol{\pi}_t) = \eta_t + \frac{\epsilon}{\pi_{i,t}}, & i = 0, \dots, n, \\ \sum_{i=0}^n \pi_{i,t} = 1. \end{cases}$$

This enforces both the barrier-based first-order conditions (FOCs) and the sum-to-one constraint.

The Jacobian $D\mathbf{F}(\boldsymbol{\pi}_t, \eta_t)$ is an $(n+2) \times (n+2)$ matrix. Ordering the unknowns as $(\pi_{0,t}, \dots, \pi_{n,t}, \eta_t)$, the rows of $D\mathbf{F}$ correspond to $(F_0, \dots, F_n, F_{\text{sum}})$. Concretely:

$$D\mathbf{F}(\boldsymbol{\pi}_t, \eta_t) = \begin{pmatrix} \frac{\partial F_0}{\partial \pi_{0,t}} & \dots & \frac{\partial F_0}{\partial \pi_{n,t}} & \frac{\partial F_0}{\partial \eta_t} \\ \vdots & \ddots & & \vdots \\ \frac{\partial F_n}{\partial \pi_{0,t}} & \dots & \frac{\partial F_n}{\partial \pi_{n,t}} & \frac{\partial F_n}{\partial \eta_t} \\ \frac{\partial F_{\text{sum}}}{\partial \pi_{0,t}} & \dots & \frac{\partial F_{\text{sum}}}{\partial \pi_{n,t}} & \frac{\partial F_{\text{sum}}}{\partial \eta_t} \end{pmatrix}.$$

Using the definitions of F_i and F_{sum} , we deduce each partial derivative. For $\frac{\partial F_i}{\partial \pi_{j,t}}$:

$$\frac{\partial F_i}{\partial \pi_{j,t}} = \frac{\partial^2 \mathcal{H}}{\partial \pi_{i,t} \partial \pi_{j,t}} - \delta_{ij} \frac{\epsilon}{\pi_{i,t}^2}, \quad 0 \leq i, j \leq n,$$

where $\frac{\partial^2 \mathcal{H}}{\partial \pi_{i,t} \partial \pi_{j,t}}$ is the second derivative of \mathcal{H} w.r.t. $\pi_{i,t}, \pi_{j,t}$, and δ_{ij} is the Kronecker delta ensuring that $-\epsilon/\pi_{i,t}^2$ appears only on the diagonal. When both $i, j \geq 1$ (risky assets), we have

$$\frac{\partial^2 \mathcal{H}}{\partial \pi_{i,t} \partial \pi_{j,t}} = (\partial_x \lambda_t^*) (X_t^*)^2 \Sigma_{ij},$$

whereas if either $i = 0$ or $j = 0$ (risk-free asset involved), then

$$\frac{\partial^2 \mathcal{H}}{\partial \pi_{i,t} \partial \pi_{j,t}} = 0.$$

For $\frac{\partial F_i}{\partial \eta_t}$:

$$\frac{\partial F_i}{\partial \eta_t} = -1, \quad 0 \leq i \leq n.$$

For F_{sum} :

$$\frac{\partial F_{\text{sum}}}{\partial \pi_{j,t}} = 1, \quad \frac{\partial F_{\text{sum}}}{\partial \eta_t} = 0, \quad 0 \leq j \leq n.$$

Assembling these partial derivatives results in an $(n+2) \times (n+2)$ system.

Solving $\mathbf{F}(\boldsymbol{\pi}_t, \eta_t) = \mathbf{0}$ can be done via Newton's method (Nocedal & Wright, 1999, Chap. 3):

$$D\mathbf{F}(\boldsymbol{\pi}_t^{(k)}, \eta_t^{(k)}) \Delta = -\mathbf{F}(\boldsymbol{\pi}_t^{(k)}, \eta_t^{(k)}), \quad \begin{pmatrix} \boldsymbol{\pi}_t^{(k+1)} \\ \eta_t^{(k+1)} \end{pmatrix} = \begin{pmatrix} \boldsymbol{\pi}_t^{(k)} \\ \eta_t^{(k)} \end{pmatrix} + \alpha_k \Delta,$$

where $0 < \alpha_k \leq 1$ is chosen (e.g., via a simple backtracking line search) so that $\pi_{i,t}^{(k+1)} > 0$. Repeating this process until $\|\mathbf{F}(\boldsymbol{\pi}_t^{(k)}, \eta_t^{(k)})\| \rightarrow 0$ yields the barrier-based solution. As $\epsilon \rightarrow 0$, it converges to the unconstrained Merton policy, except for any $\pi_{i,t}$ pinned near zero.

The barrier-based procedure provides a stable, scalable way to enforce $\pi_{i,t} \geq 0$ and $\sum_{i=0}^n \pi_{i,t} = 1$ in large-scale continuous-time portfolio problems. It avoids the heavy cost of KKT-based active-set methods while maintaining positivity and scalability. A moderate ϵ balances strict positivity with computational tractability, as very small ϵ approximates the exact inequality constraints but risks ill-conditioning. Sparse or iterative solvers can mitigate costs for large n , making this approach practical for high-dimensional settings.

3.3 Policy-Fixed Adjoint Processes and Parameter Gradients

In neural network implementations, suboptimal policies $(\boldsymbol{\pi}_\theta, C_\phi)$ can still induce well-defined adjoint processes through an *augmented* Hamiltonian $\tilde{\mathcal{H}}$ as in (10)

and (20). This Hamiltonian subsumes both the standard Pontryagin structure and any constraint mechanisms (e.g., KKT multipliers or barrier terms). Formally, the *policy-fixed adjoint* $(\lambda_t, \mathbf{Z}_t)$ satisfies the backward stochastic differential equation (BSDE):

$$\begin{aligned} d\lambda_t &= - \frac{\partial}{\partial X} \tilde{\mathcal{H}}(t, X_t, \boldsymbol{\pi}_\theta(t, X_t), C_\phi(t, X_t), \lambda_t, \mathbf{Z}_t) dt + \mathbf{Z}_t^\top d\mathbf{W}_t, \\ \lambda_T &= \frac{\partial}{\partial X} \left[\kappa e^{-\rho T} U(X_T) \right], \end{aligned} \quad (12)$$

where X_t evolves under the *suboptimal* policy $(\boldsymbol{\pi}_\theta, C_\phi)$. This stands in contrast to the *optimal* adjoint processes $(\lambda_t^*, \mathbf{Z}_t^*)$ in (6), which are associated with the true optimal controls $(\boldsymbol{\pi}_t^*, C_t^*)$. The suboptimal adjoint $(\lambda_t, \mathbf{Z}_t)$ thus quantifies local sensitivities relative to the parameterized (possibly non-optimal) controls.

When constraints are added (e.g., no short-selling, consumption bounds), we *augment* the original Hamiltonian as

$$\tilde{\mathcal{H}} = \mathcal{H} + (\text{barrier/KKT/etc. terms}).$$

While these additive terms change the *content* of $\tilde{\mathcal{H}}$, they do not alter the structural form of the backward equation (12). Mathematically, the adjoint SDE depends only on the first-order derivative $\partial \tilde{\mathcal{H}} / \partial X$, which remains well-defined regardless of how constraints are imposed. This unification allows both unconstrained and constrained problems to be handled consistently within a single theoretical framework.

Modern deep learning frameworks (e.g., PyTorch) do *not* numerically solve (12) directly. Instead, they leverage the fact that the adjoint process λ_t represents the sensitivity of the performance functional J , defined in (2), with respect to the state X_t :

$$\lambda_t = \frac{\partial J}{\partial X_t}.$$

This quantity is computed automatically via backpropagation through the computational graph of X_t . Once λ_t is obtained, the process \mathbf{Z}_t can be recovered through an additional relation (8), which links $\partial_x \lambda_t$ to \mathbf{Z}_t via the policy-driven diffusion. As a result, $(\lambda_t, \mathbf{Z}_t)$ emerge as byproducts of the gradient calculation $\nabla_{\theta, \phi} J$, bypassing the need for a standalone BSDE solver and significantly simplifying the time discretization process.

We now define the *network-based* objective, $J(\theta, \phi)$, as an approximation of (2) that employs the neural-network controls $(\boldsymbol{\pi}_\theta, C_\phi)$. Then, the parameter gradients

adopt a Pontryagin-like form (see Ma & Yong, 1999; Yong & Zhou, 2012):

$$\nabla_{\theta} J = \mathbb{E} \left[\int_0^T \left(\lambda_t \frac{\partial b}{\partial \theta} + \mathbf{Z}_t^{\top} \frac{\partial \sigma}{\partial \theta} \right) dt \right] + (\text{direct payoff term in } \theta), \quad (13)$$

$$\nabla_{\phi} J = \mathbb{E} \left[\int_0^T \left(\lambda_t \frac{\partial b}{\partial \phi} + \mathbf{Z}_t^{\top} \frac{\partial \sigma}{\partial \phi} \right) dt \right] + (\text{direct payoff term in } \phi). \quad (14)$$

Here, λ_t and \mathbf{Z}_t are precisely the *policy-fixed* adjoint processes from (12), while b and σ denote the drift and diffusion of X_t under $(\boldsymbol{\pi}_{\theta}, C_{\phi})$.

Following Section 2.1, let

$$b(t, X_t, \boldsymbol{\pi}_t, C_t) = X_t \boldsymbol{\pi}_t^{\top} \tilde{\boldsymbol{\mu}}_t - C_t, \quad \sigma(t, X_t, \boldsymbol{\pi}_t) = X_t \boldsymbol{\pi}_t^{\top} \tilde{V}_t,$$

where $\tilde{\boldsymbol{\mu}}_t \in \mathbb{R}^{n+1}$ collects the risk-free rate r_t and the n risky drifts $\mu_{i,t}$, while $\tilde{V}_t \in \mathbb{R}^{(n+1) \times n}$ encodes a zero row for the risk-free asset plus the factorization V_t of Σ_t . Defining $\boldsymbol{\pi}_t = \boldsymbol{\pi}_{\theta}(t, X_t)$ and $C_t = C_{\phi}(t, X_t)$, the partial derivatives become:

$$\frac{\partial b}{\partial \theta} = X_t \tilde{\boldsymbol{\mu}}_t^{\top} \frac{\partial \boldsymbol{\pi}_{\theta}}{\partial \theta}, \quad \frac{\partial b}{\partial \phi} = -\frac{\partial C_{\phi}}{\partial \phi}, \quad \frac{\partial \sigma}{\partial \theta} = X_t \tilde{V}_t^{\top} \frac{\partial \boldsymbol{\pi}_{\theta}}{\partial \theta}, \quad \frac{\partial \sigma}{\partial \phi} = 0.$$

Additionally, the direct utility of consumption $\int_0^T e^{-\rho t} U(C_{\phi}(t, X_t)) dt$ contributes

$$\frac{\partial}{\partial \phi} \left[e^{-\rho t} U(C_{\phi}(t, X_t)) \right] = e^{-\rho t} U'(C_{\phi}(\cdot)) \frac{\partial C_{\phi}(\cdot)}{\partial \phi}.$$

Substituting into (13)–(14) yields the *expanded* expressions:

$$\nabla_{\theta} J = \mathbb{E} \left[\int_0^T \left\{ \lambda_t X_t \tilde{\boldsymbol{\mu}}_t + X_t (\tilde{V}_t^{\top} \mathbf{Z}_t) \right\}^{\top} \frac{\partial \boldsymbol{\pi}_{\theta}}{\partial \theta} dt \right], \quad (15)$$

$$\nabla_{\phi} J = \mathbb{E} \left[\int_0^T \lambda_t \left(-\frac{\partial C_{\phi}}{\partial \phi} \right) dt \right] + \mathbb{E} \left[\int_0^T e^{-\rho t} U'(C_{\phi}(\cdot)) \frac{\partial C_{\phi}(\cdot)}{\partial \phi} dt \right]. \quad (16)$$

Because $\frac{\partial \sigma}{\partial \phi} = 0$ in this Merton-like setup, the consumption gradient has two clear terms: a *wealth sensitivity* part ($-\lambda_t \partial_{\phi} C_{\phi}$) and a *direct utility* part ($e^{-\rho t} U'(C_{\phi}) \partial_{\phi} C_{\phi}$).

Equations (15)–(16) illustrate how the adjoint variables $(\lambda_t, \mathbf{Z}_t)$, obtained via automatic differentiation, dictate the directions to update (θ, ϕ) . As $(\boldsymbol{\pi}_{\theta}, C_{\phi})$ approach the Hamiltonian maximizer under $\tilde{\mathcal{H}}$, these gradients vanish, recovering classical Merton solutions (unconstrained) or constrained analogs (when barrier/KKT terms are present). Thus, neural network training aligns with Pontryagin’s principle, without requiring explicit BSDE solvers. Under standard Lipschitz/integrability assumptions, this approach readily scales to large-scale portfolios while retaining theoretical consistency.

4 Gradient-Based Algorithm for Policy Optimization

Thus far, we have shown how Pontryagin’s Maximum Principle (PMP) provides a forward–backward characterization of the optimal solution in both *unconstrained* and *constrained* (high-dimensional) Merton problems. However, translating these continuous-time PMP conditions into practice requires numerical approximations. We adopt a *gradient-based* scheme that leverages backpropagation through time (BPTT) to iteratively refine a neural-network policy. This approach extends the one-dimensional methods of Huh (2024)—who introduced the PG-DPO algorithm in a 1D Merton setting—to accommodate *multi-asset* portfolios, as well as the *barrier* framework for enforcing nonnegative weights and sum-to-one constraints.

Concretely, we parametrize both the *consumption* and *investment* decisions by neural networks, then compute a suboptimal *costate* (adjoint) process via BPTT under the current policy parameters. This costate informs how to adjust the policy in each gradient step to reduce the discrepancy between the induced Hamiltonian and its local Pontryagin maximum. In the *unconstrained* case, the training simply proceeds via direct policy gradients, while in the *constrained* case, we embed constraints through network activations (e.g. softmax for nonnegative weights).

Additionally, we introduce a *OneShot* procedure that directly extracts near-optimal Pontryagin controls from the BPTT-derived adjoint, potentially bypassing further policy training at test time. Specifically, if the adjoint $(\lambda_t, \mathbf{Z}_t)$ converges quickly, one can deploy “OneShot” Pontryagin rules (either a closed-form formula in unconstrained Merton or a barrier-based Newton step in the constrained case), thus ignoring the network outputs at inference. This can significantly reduce the total training overhead for large-scale portfolios.

Hence, the methods in this section form a *Pontryagin-Guided Direct Policy Optimization (PG-DPO)* family with two main variants:

- **PG-DPO** (baseline), which trains the neural policy end-to-end and deploys it directly (Section 4.2).
- **PG-DPO-OneShot**, which relies on a brief “warm-up” training phase, then applies Pontryagin controls via a closed-form or barrier-based solve at test time (Section 4.3).

Compared to classical dynamic programming or PDE grids, both PG-DPO variants are readily scalable to multi-asset, high-dimensional settings, thanks to efficient BPTT and GPU implementations. In the remainder of this section, we detail how the forward–backward neural policy training works (§4.2), and how the OneShot procedure integrates with unconstrained or barrier-based constraints (§4.3).

4.1 Single-Path Approach for Estimating Adjoint Processes

A key insight of our method is that one forward simulation (or single path) can produce an unbiased estimate of the adjoint processes λ_t and \mathbf{Z}_t at the visited time-state points (t_k, X_k) . Specifically, $\lambda_t = \frac{\partial J}{\partial X_t}$ captures how marginal variations in the scalar wealth process X_t affect the objective $J(\boldsymbol{\pi}_t, C_t)$. In a *multi-asset* setting, $\mathbf{Z}_t \in \mathbb{R}^n$ similarly encodes how the noise directions in \mathbf{W}_t propagate through the policy’s diffusion terms. Once we differentiate the policy networks and the forward simulation via automatic differentiation, we can retrieve consistent estimates of λ_t and \mathbf{Z}_t by backpropagating from the scalar objective $J(\boldsymbol{\pi}_t, C_t)$. Although the precise mapping between λ_t, \mathbf{Z}_t and the policy variables can differ across problem dimensions and parameterizations of Σ , the overarching idea remains: a single trajectory suffices to yield a pathwise (unbiased) estimate of the adjoint processes at each point (t_k, X_k) .

This single-path approach has several attractive properties. First, it is unbiased in the sense that, over many random draws, the average of the estimated adjoints converges to the true costates in expectation (Kushner & Yin, 2003; Borkar & Borkar, 2008). Second, it is memory-efficient because each node (t_k, X_k) is visited by exactly one trajectory (or one mini-batch), avoiding the need to store large datasets or ensembles. Third, it is online-adaptive in that, as θ, ϕ are updated, new samples are drawn in real time, ensuring the policy remains well-trained for the state distribution induced by its latest parameters.

On the other hand, using only a single sample per node can lead to higher variance in gradient estimates, potentially slowing or destabilizing learning. Section 4.3 shows how we can leverage the adjoint estimates directly through a *OneShot* approach, bypassing the learned policy for faster inference if needed.

4.2 Discrete-Time Algorithm for Gradient Computation

We now detail a concrete procedure, in discrete time, for computing both the adjoint processes $(\lambda_t, \mathbf{Z}_t)$ and the parameter gradients $(\nabla_{\theta} J, \nabla_{\phi} J)$ under the multi-asset Merton model. This algorithm implements backpropagation-through-time (BPTT), jointly handling consumption and multi-dimensional investment decisions. Concretely, the following steps outline the core of our PG-DPO approach in discrete time:

(a) Choose Final Activations for Network Constraints. When designing the neural networks $\boldsymbol{\pi}_{\theta}$ and C_{ϕ} , one can *directly* enforce constraints on the controls via their final-layer activations:

- *Unconstrained:* Simply output real-valued coordinates; no explicit activation is needed.

- *No Borrowing / Short-Selling*: Use a softmax of length $n+1$ to ensure $\boldsymbol{\pi}_k \geq \mathbf{0}$ and $\sum_{i=0}^n \pi_{i,k} = 1$.
- *Consumption Bounds*: If $0 \leq C_k \leq \alpha X_k$ must hold, a scaled sigmoid final activation can keep C_k within that range.

Such architectural choices make the policy outputs automatically satisfy their respective constraints at each time step, minimizing the need for separate penalty or barrier terms.

(b) Discretize Dynamics and Objective. Partition the time interval $[0, T]$ into N steps of size $\Delta t = T/N$. Define $t_k = k \Delta t$ for $k = 0, \dots, N$, so that $t_0 = 0$ and $t_N = T$. We approximate the continuous-time SDE in (1) via an *exponential Euler* scheme that preserves the geometric nature of wealth updates. Concretely, we *freeze* the controls $(\boldsymbol{\pi}_t, C_t)$ on each interval $[t_k, t_k + \Delta t]$. Here we let

$$\boldsymbol{\pi}_k = \boldsymbol{\pi}_\theta(t_k, X_k), \quad C_k = C_\phi(t_k, X_k).$$

Applying Itô's lemma to $\ln(X_s)$ over $[t_k, t_k + \Delta t]$ yields the local exponential solution

$$X_{k+1} = X_k \exp\left(\left[\boldsymbol{\pi}_k^\top \tilde{\boldsymbol{\mu}}_k - \frac{1}{2} \boldsymbol{\pi}_{1:n,k}^\top \Sigma_k \boldsymbol{\pi}_{1:n,k} - \frac{C_k}{X_k}\right] \Delta t + \boldsymbol{\pi}_k^\top \tilde{V}_k \Delta \mathbf{W}_k\right),$$

where $\boldsymbol{\pi}_{1:n,k}$ is the sub-vector $(\pi_{1,k}, \dots, \pi_{n,k})$, $\Sigma_k = V_k V_k^\top$, and $\Delta \mathbf{W}_k = \mathbf{W}_{t_k + \Delta t} - \mathbf{W}_{t_k} \sim \mathcal{N}(\mathbf{0}, \Delta t I_n)$. As before, $\tilde{\boldsymbol{\mu}}_k \in \mathbb{R}^{n+1}$ collects $(r_{t_k}, \mu_{1,t_k}, \dots, \mu_{n,t_k})$, and $\tilde{V}_k \in \mathbb{R}^{(n+1) \times n}$ encodes a zero row for the risk-free asset plus the factorization of Σ_k . This exponential step can be iterated to approximate the continuous-time dynamics. Our goal is to choose parameters (θ, ϕ) so as to maximize $J(\theta, \phi)$.

(c) Single Forward Path per (t_k, X_k) . At each node (t_k, X_k) , we run exactly one forward simulation from k to the terminal index N . This yields a single-sample payoff, unbiased but subject to Monte Carlo variance. After the simulation, backpropagation (autodiff) yields local adjoint estimates λ_k and \mathbf{Z}_k under the current policy (θ, ϕ) .

(d) Compute λ_k via BPTT. In typical deep-learning frameworks (e.g., PyTorch or JAX), we build a computational graph from (θ, ϕ) through $\{\boldsymbol{\pi}_k, C_k\}$ and $\{X_k\}$ to the approximate objective $J(\theta, \phi)$. A single call to `.backward()` (or an equivalent AD routine) computes $\nabla_\theta J$ and $\nabla_\phi J$, as well as the partial derivatives of J w.r.t. each X_k . Identifying

$$\lambda_k = \frac{\partial J}{\partial X_k}$$

aligns with the Pontryagin perspective that λ_k is the (suboptimal) adjoint measuring the sensitivity of the overall cost to changes in X_k .

(e) Obtain $\partial_x \lambda_k$ and hence \mathbf{Z}_k . To compute \mathbf{Z}_k , one typically needs $\partial_x \lambda_k$. In the multi-asset zero-indexed Merton model, a common approach differentiates the Hamiltonian or uses the relation

$$\mathbf{Z}_k \approx [\partial_x \lambda_k] \left(X_k \tilde{V}_k^\top \boldsymbol{\pi}_k \right).$$

Although this step does not *impose* optimality, it provides additional derivatives needed for constructing the exact parameter gradients (cf. (13)–(14)).

(f) Update Network Parameters. Finally, we collect $\nabla_\theta J$ and $\nabla_\phi J$ and update (θ, ϕ) using a stochastic optimizer (e.g., Adam or SGD). In discrete time, one typically sums the integrands over $k = 0, \dots, N - 1$ with a factor of Δt . For instance, the expanded $\nabla_\theta J$ might be approximated by

$$\nabla_\theta J \approx \mathbb{E} \left[\sum_{k=0}^{N-1} \left\{ \lambda_k X_k \tilde{\boldsymbol{\mu}}_k + X_k (\tilde{V}_k \mathbf{Z}_k) \right\}^\top \frac{\partial \boldsymbol{\pi}_\theta(t_k, X_k)}{\partial \theta} \Delta t \right], \quad (17)$$

while the expanded $\nabla_\phi J$ might be approximated by

$$\nabla_\phi J \approx \mathbb{E} \left[\sum_{k=0}^{N-1} \lambda_k \left(-\frac{\partial C_\phi(t_k, X_k)}{\partial \phi} \right) \Delta t \right] + \mathbb{E} \left[\sum_{k=0}^{N-1} e^{-\rho t_k} U'(C_k) \frac{\partial C_\phi(t_k, X_k)}{\partial \phi} \Delta t \right]. \quad (18)$$

Averaging these over M trajectories (or mini-batches) yields a stochastic approximation of $\nabla_\theta J$ and $\nabla_\phi J$. Repeating this process eventually produces a stationary policy.

In practice, one could simply define the neural policy $(\boldsymbol{\pi}_\theta, C_\phi)$, compute $J(\theta, \phi)$ on simulated trajectories, and call `.backward()`; automatic differentiation then handles the internal adjoint logic. Nonetheless, explicitly recognizing $(\lambda_k, \mathbf{Z}_k)$ as suboptimal Pontryagin adjoints clarifies why backpropagation works and how to incorporate additional alignment or constraints. Altogether, these steps form the foundation of our PG-DPO scheme in the multi-asset Merton setting.

4.3 OneShot PG-DPO with BPTT-Derived Adjoint

One key insight of our approach is that the adjoint (costate) process λ_t and its derivative $\partial_x \lambda_t$ can converge relatively quickly under backpropagation-through-time (BPTT), even if the policy networks $(\boldsymbol{\pi}_\theta, C_\phi)$ remain suboptimal. This observation motivates a *OneShot* procedure, which derives near-optimal controls $(\boldsymbol{\pi}^{\text{PMP}}, C^{\text{PMP}})$ directly from $(\lambda_t, \partial_x \lambda_t)$, thereby bypassing the neural-network outputs at test time. Below, we outline how this works in both *unconstrained* and *constrained* settings.

(a) Unconstrained OneShot. If the problem imposes *no* constraints on borrowing or consumption, the adjoint $(\lambda_k, \partial_x \lambda_k)$ can be plugged into a closed-form Pontryagin solution. One obtains the continuous-time first-order conditions (7) and (9) from Pontryagin’s Maximum Principle. When these expressions are *discretized* in time, they yield a rule such as

$$\begin{aligned} C_k^{\text{PMP}} &= \left(e^{\rho t_k} \lambda_k \right)^{-\frac{1}{\gamma}}, \\ \boldsymbol{\pi}_{1:n,k}^{\text{PMP}} &= -\frac{\lambda_k}{X_k (\partial_x \lambda_k)} \Sigma_k^{-1} (\mu_{1,k} - r_k, \dots, \mu_{n,k} - r_k). \end{aligned} \quad (19)$$

Hence, once BPTT has produced sufficiently accurate $\lambda_k \approx \frac{\partial J}{\partial X_k}$ and $\partial_x \lambda_k$, we can immediately compute $(\boldsymbol{\pi}_k^{\text{PMP}}, C_k^{\text{PMP}})$ *in one shot* without further network training. This approach can dramatically reduce computational cost if (19) is available.

(b) Constrained OneShot (Barrier Method). In the presence of constraints (e.g., no short-selling or consumption bounds), we no longer have a simple closed-form from the Pontryagin FOCs. Moreover, a KKT-based method can be computationally expensive due to large, piecewise systems. Instead, we adopt a *barrier-based* approach, quickly solving a small-scale system at each node $(t_k, X_k, \lambda_k, \partial_x \lambda_k)$. Recall the *barrier* Hamiltonian

$$\tilde{\mathcal{H}}_{\text{barrier}} = \mathcal{H} + \eta_t \left(1 - \sum_{i=0}^n \pi_{i,t} \right) + \epsilon \sum_{i=0}^n \ln(\pi_{i,t}), \quad (20)$$

where η_t enforces $\sum_{i=0}^n \pi_{i,t} = 1$ and the log-barrier $\epsilon \sum_{i=0}^n \ln(\pi_{i,t})$ ensures $\pi_{i,t} > 0$. Once BPTT provides λ_k and $\partial_x \lambda_k$, we incorporate them into $\tilde{\mathcal{H}}_{\text{barrier}}$ and *locally* solve $\max_{\boldsymbol{\pi}_k, C_k} \tilde{\mathcal{H}}_{\text{barrier}}$ (e.g., via Newton–line-search of Section 3.2.2) to obtain $(\boldsymbol{\pi}_k^{\text{PMP}}, C_k^{\text{PMP}})$. Because this is only a low-dimensional solve (roughly $n + 2$ if we count the multiplier η_t), it is typically much faster than retraining the entire network. Thus, even with constraints, we can treat λ_k and $\partial_x \lambda_k$ as a “shortcut” for computing OneShot controls at each (t_k, X_k) .

(c) Workflow of OneShot. In practice, we proceed as follows:

1. *Warm up:* Partially train $(\boldsymbol{\pi}_\theta, C_\phi)$ so that λ_t and \mathbf{Z}_t become reasonably stable under BPTT.
2. *Extract:* On the desired test scenario, forward-simulate to obtain λ_k, \mathbf{Z}_k at each node (t_k, X_k) .
3. *Compute OneShot Controls:*
 - *Unconstrained:* Use a closed-form FOC (19) if available.

- *Constrained*: Solve the barrier system (20) to find $(\boldsymbol{\pi}_k^{\text{PMP}}, C_k^{\text{PMP}})$.
4. *Deploy*: The resulting $(\boldsymbol{\pi}_k^{\text{PMP}}, C_k^{\text{PMP}})$ can be used at test time, ignoring the original policy network outputs. In many cases, this drastically reduces the remaining training cost while still achieving near-optimal performance.

Although OneShot does not produce a final policy network for direct deployment, it remains highly flexible. Indeed, one can simply run a brief forward pass and backprop for each new initial state, using costate-based formulas or barrier solves to generate near-optimal controls without further network updates. Numerical experiments (Section 5) confirm that OneShot can substantially reduce training effort, achieving near-optimal performance even with a moderate warm-up phase, whether constraints are present or not.

4.4 Extended Value Function and Algorithmic Variants

4.4.1 Extended Value Function and Discretized Rollouts

In Section 4.2, we introduced a discretization scheme for the Merton problem over a fixed interval $[0, T]$. Here, we extend that approach to handle any initial time t_0 and wealth x_0 by defining an extended value function over a broader domain.

Many continuous-time problems (including Merton) require a policy $(\boldsymbol{\pi}_\theta, C_\phi)$ valid for any initial condition (t_0, x_0) . To address this requirement, we define an *extended value function* that integrates over random initial nodes $(t_0, x_0) \sim \eta(\cdot)$ in the domain $\mathcal{D} \subset [0, T] \times (0, \infty)$, and then discretize each resulting trajectory. Here, η denotes the distribution of (t_0, x_0) . Concretely, we set

$$\widehat{J}(\theta, \phi) = \mathbb{E}_{(t_0, x_0) \sim \eta} \left[\mathbb{E} \left(\int_{t_0}^T e^{-\rho u} U(C_\phi(u, X_u)) du + \kappa e^{-\rho T} U(X_T) \right) \right].$$

Hence, maximizing $\widehat{J}(\theta, \phi)$ yields a policy $(\boldsymbol{\pi}_\theta, C_\phi)$ that applies across all sub-intervals $[t_0, T]$ and initial wealth x_0 .

To avoid overfitting to a single initial scenario, we draw (t_0, x_0) from a suitable distribution η . By doing so, the policy $(\boldsymbol{\pi}_\theta, C_\phi)$ is trained to cover a broad region of the time–wealth domain rather than just one initial condition. This sampling strategy is standard in many PDE-based or RL-like continuous-time methods that need a single control law $(\boldsymbol{\pi}_\theta, C_\phi)$ covering all (t, x) .

To implement the integral in $\widehat{J}(\theta, \phi)$, one can follow the step-by-step procedure in Algorithm 1, which details how to discretize the interval, simulate each path, and apply backpropagation to update (θ, ϕ) .

4.4.2 Gradient-Based Algorithmic Variants

Having introduced the extended value function $\widehat{J}(\theta, \phi)$ over random initial nodes (t_0, x_0) , we now present two main PG-DPO methods for the multi-asset Merton problem. Both rely on the same procedure of simulating from sampled initial conditions and computing a stochastic estimate of $\widehat{J}(\theta, \phi)$. They differ in whether we *deploy the learned networks* or a *one-shot Pontryagin control* at test time. When constraints such as no short-selling or consumption bounds are present, we handle them either by final-layer activations in the policy nets (Section 4.2) or by a barrier-based one-shot solution (Sections 3.2.2 and 4.3).

(a) **PG-DPO (Baseline).**

This is the *basic* scheme, analogous to Algorithm 1. It optimizes \widehat{J} directly via backpropagation-through-time (BPTT), returning a final policy (π_θ, C_ϕ) . In unconstrained settings, the network can produce any real values; in constrained scenarios (e.g. sum-to-one, no negative weights), we can enforce them with softmax or scaled sigmoids. Empirically, PG-DPO converges reliably toward Pontryagin-like solutions, albeit with potentially slower or noisier training as dimension grows.

(b) **PG-DPO-OneShot.**

A second variant uses the fact that the costate (adjoint) λ_t may converge faster than the policy networks themselves. After a short warm-up phase (running PG-DPO for a few iterations), we extract $\lambda_k \approx \frac{\partial J}{\partial X_k}$ and $\partial_x \lambda_k$ from BPTT. We then compute $(\pi_k^{\text{PMP}}, C_k^{\text{PMP}})$ using either a *closed-form Pontryagin rule* (unconstrained Merton) or a *barrier-based Newton solve* (§3.2.2). At test time, we *ignore* the neural-network outputs and directly deploy those one-shot Pontryagin controls. This drastically reduces training requirements by bypassing final network inference, though it does not produce a “ready-to-deploy” policy net for real-time usage.

Both methods extend naturally to the multi-asset case by leveraging Pontryagin’s principle (Section 3.3) and the barrier approach if constraints are involved (Section 3.2.2). One typically samples (t_0, x_0) from a chosen distribution η to cover various times and wealth levels, and then computes λ_0 (and $\frac{\partial \lambda_0}{\partial x}$) for each sample. A detailed proof of convergence in a single-asset setting can be found in Huh (2024); although restricted to one dimension, it extends to multi-asset problems under mild assumptions (e.g. Lipschitz continuity of drift/diffusion, differentiability of the policy nets).

Algorithm 1 PG-DPO

Inputs:

- Policy nets $(\boldsymbol{\pi}_\theta, C_\phi)$ (optionally with constraint-enforcing final activations);
- Step sizes $\{\alpha_k\}$, total iterations K ;
- Domain sampler η for $(t_0^{(i)}, x_0^{(i)})$ in $\mathcal{D} \subset [0, T] \times (0, \infty)$;
- Integer N (steps per path).

1: **for** $j = 1$ to K **do**

2: **(a) Sample mini-batch of size M .** For each $i \in \{1, \dots, M\}$, draw $(t_0^{(i)}, x_0^{(i)}) \sim \eta$.

3: **(b) Local Single-Path Simulation.** For each i :

(a) $\Delta t^{(i)} \leftarrow \frac{T-t_0^{(i)}}{N}$; $X_0^{(i)} \leftarrow x_0^{(i)}$.

(b) For $k = 0, \dots, N-1$:

$$\boldsymbol{\pi}_k^{(i)} = \boldsymbol{\pi}_\theta(t_k^{(i)}, X_k^{(i)}), C_k^{(i)} = C_\phi(t_k^{(i)}, X_k^{(i)}),$$

$$X_{k+1}^{(i)} = X_k^{(i)} \exp\left(\left[\left(\boldsymbol{\pi}_k^{(i)}\right)^\top \tilde{\boldsymbol{\mu}}_k^{(i)} - \frac{1}{2} \left(\boldsymbol{\pi}_{1:n,k}^{(i)}\right)^\top \Sigma_k^{(i)} \boldsymbol{\pi}_{1:n,k}^{(i)} - \frac{C_k^{(i)}}{X_k^{(i)}}\right] \Delta t^{(i)} + \left(\boldsymbol{\pi}_k^{(i)}\right)^\top \tilde{V}_k^{(i)} \Delta \mathbf{W}_k^{(i)}\right).$$

(c) Compute

$$J^{(i)}(\theta, \phi) = \sum_{k=0}^{N-1} e^{-\rho t_k^{(i)}} U(C_k^{(i)}) \Delta t^{(i)} + \kappa e^{-\rho T} U(X_N^{(i)}).$$

4: **(c) Backprop & Averaging:**

$$\hat{J}(\theta, \phi) = \frac{1}{M} \sum_{i=1}^M J^{(i)}(\theta, \phi), \quad \nabla_{(\theta, \phi)} \hat{J} \leftarrow \text{BPTT}.$$

5: **(d) Parameter Update:**

$$(\theta, \phi) \leftarrow (\theta, \phi) + \alpha_k \nabla_{(\theta, \phi)} \hat{J}.$$

6: **end for**

7: **return** $(\boldsymbol{\pi}_\theta, C_\phi)$.

Algorithm 2 PG-DPO-OneShot

Additional Inputs:

- A brief “warm-up” phase (e.g., K_0 iterations of PG-DPO).
 - Suboptimal adjoint λ_k and its spatial derivative $\frac{\partial}{\partial x}\lambda_k$, *both* obtained via automatic differentiation (BPTT) for each node (t_k, X_k) .
- 1: **(a) Warm-Up Training:**
 - (a) Run PG-DPO for K_0 iterations. Although π_θ, C_ϕ may remain suboptimal, the costate $\lambda_t \approx \frac{\partial J}{\partial X_t}$ typically stabilizes quickly under BPTT.
 - (b) After warm-up, at each node (t_k, X_k) , retrieve λ_k and $\frac{\partial}{\partial x}\lambda_k$ from autodiff.
 - 2: **(b) OneShot Pontryagin Controls (Unconstrained vs. Barrier).**
 - (a) *If unconstrained*, apply a closed-form Pontryagin FOC $(\pi_k^{\text{PMP}}, C_k^{\text{PMP}})$ (e.g. (19) in a multi-asset Merton model).
 - (b) *If constraints exist*, solve $\max_{\pi_k, C_k} \tilde{\mathcal{H}}_{\text{barrier}}$ (see (20)) via a small-scale *barrier-based* Newton–line-search at $(t_k, X_k, \lambda_k, \frac{\partial}{\partial x}\lambda_k)$. Return $(\pi_k^{\text{PMP}}, C_k^{\text{PMP}})$.
 - 3: **(c) Deploy OneShot Controls:**
 - (a) At test time, *ignore* the network outputs (π_θ, C_ϕ) . Use $(\pi_k^{\text{PMP}}, C_k^{\text{PMP}})$ from step (c) instead.
 - (b) This requires only a short warm-up plus local solves (closed-form or barrier). Experiments (Section 5) confirm near-optimal solutions with significantly reduced training cost.
-

5 Numerical Results

In this section, we illustrate how our Pontryagin-Guided Direct Policy Optimization (PG-DPO) framework applies to a *multi-asset* Merton problem that integrates both portfolio allocation and continuous consumption. While many recent deep learning approaches to stochastic control—including deep BSDE methods (e.g., Han et al., 2018; Weinan, 2017), physics-informed neural networks (Raissi et al., 2019), and model-free reinforcement learning (e.g., Reppen et al., 2023; Reppen & Soner, 2023; Dai et al., 2023)—have shown promise in lower-dimensional or simpler PDE settings, we focus on the large-scale, continuous-time setting with potentially

thousands of risky assets.

We consider two main scenarios. First, in Section 5.2, we examine the *standard Merton problem* under an *unconstrained* setting with constant drift and volatility (i.e., a constant opportunity set). In this classical setup, a *closed-form solution* is well-known to exist, which allows us to directly compare PG-DPO and its one-shot variant against the analytical optimum as the number of risky assets grows. Second, in Section 5.3, we add *no short-selling or borrowing* constraints. Because no closed-form solution is available under these constraints, we measure the residual in the first-order optimality conditions (FOCs) as our accuracy metric. Before discussing each scenario in detail, Section 5.1 describes our experimental setup, including parameter choices, neural network architectures, and training procedures.

5.1 Experimental Setup

We consider an investment horizon up to $T = 1$ and confine the wealth domain to $[0.1, 2]$. In all our experiments, the *drift* $\boldsymbol{\mu}_t$ and *covariance* Σ_t of the risky asset returns are *constant over time*, i.e., $\boldsymbol{\mu}_t = \boldsymbol{\mu}$ and $\Sigma_t = \Sigma$ for all $0 \leq t \leq T$. This ensures that the underlying wealth dynamics follow a standard geometric Brownian motion with time-invariant parameters, making the classical Merton closed-form solution applicable in the *unconstrained* case (see Section 2.3). Nonetheless, once constraints (e.g., no short-selling or borrowing) are introduced, a closed-form solution generally ceases to exist, which motivates the numerical methods developed in this study.

For each multi-asset scenario, the number of risky assets (denoted by n) can take values in $\{10, 100, 1000, 10000\}$. To obtain stable yet varied sets of market parameters $(\boldsymbol{\mu}, \Sigma)$, we adopt a random-correlation-based procedure: we first generate a random correlation matrix, then scale it to reflect different levels of volatility, and finally sample the drift vector $\boldsymbol{\mu}$ from a prescribed distribution. This approach yields a broad range of possible market environments while preserving the time-invariance of $\boldsymbol{\mu}$ and Σ .

- (a) **Correlation and Volatility.** We first generate a positive-definite correlation matrix $\mathbf{C} \in \mathbb{R}^{n \times n}$ (ensuring unit diagonal) and draw each asset’s volatility σ_i from $[\nu_{\min}, \nu_{\max}] = [0.05, 0.5]$. We then form the covariance matrix Σ by

$$\Sigma = \text{diag}(\boldsymbol{\sigma}) \mathbf{C} \text{diag}(\boldsymbol{\sigma}),$$

thereby controlling both volatility and correlation in a realistic range.

- (b) **Baseline Portfolio Constraints.** We generate an initial portfolio $\boldsymbol{\pi} = (\pi_1, \dots, \pi_n) \in \mathbb{R}^n$ by sampling each component π_i from $[\pi_{\min}, \pi_{\max}]$, where

$\pi_{\min} = -1.0$ and $\pi_{\max} = 2.0$. Let

$$s = \sum_{i=1}^n \pi_i.$$

If s lies outside a target interval $[s_{\min}, s_{\max}]$ (for example $[0.2, 0.75]$), we rescale π so that its new sum remains within $[s_{\min}, s_{\max}]$. Concretely,

$$\pi \leftarrow \pi \times \frac{\alpha}{s}, \quad \text{where } \alpha = \begin{cases} s_{\min}, & \text{if } s < s_{\min}, \\ s_{\max}, & \text{if } s > s_{\max}. \end{cases}$$

This prevents degenerate portfolios, e.g. those with overly high leverage $\sum_i \pi_i \gg 1$ or near-zero exposure $\sum_i \pi_i \approx 0$.

(c) **Drift Vector.** Finally, each asset's drift μ_i is defined by

$$\mu_i = r + \gamma \sum_{j=1}^n \Sigma_{i,j} \pi_j, \quad i = 1, \dots, n,$$

where $r = 0.03$ is the risk-free rate and $\gamma = 2.0$ is a risk-aversion parameter. For the large-scale case ($n = 1000$), we fix a random seed (e.g., 42) to ensure reproducibility. This setup keeps Σ in a moderate range while preventing the baseline portfolio π from becoming extreme or trivial.

In addition, we set a discount rate $\rho = 0.1$ in the objective and choose $\varepsilon = 0.1$ for any noise scaling (when applicable). We allow up to $m = 5$ simulation steps per rollout. As mentioned before, the maximum time horizon is $T_{\max} = 1$, with wealth restricted to $[0.1, 2]$. Typically, we sample 10^3 initial states (t_0, X_0) at each training iteration, drawing each pair uniformly from $[0, T_{\max}] \times [0.1, 2]$. For each sampled initial pair, we set the local time step $\Delta t = (T_{\max} - t_0)/m$ and perform Euler–Maruyama updates to simulate forward to time T_{\max} . All MSE results reported in subsequent subsections are computed by repeatedly sampling these (t_0, X_0) pairs, simulating under the current policy, and then comparing the resulting (C_t, π_t) to the known solution (unconstrained case of Section 5.2) or measuring FOC residuals (constrained case of Section 5.3).

We define two neural networks, C_ϕ and π_θ , to parameterize the consumption and investment strategies, respectively. Both networks consist of two hidden layers with 200 nodes each, using Leaky-ReLU activation functions. For the consumption network C_ϕ , a softplus activation is applied in the final layer to ensure that the outputs are strictly nonnegative.

In the unconstrained case, the investment network π_θ outputs real-valued coordinates in \mathbb{R}^n without any final activation. In the constrained case, the network

enforces no short-selling or borrowing by using a softmax final layer, which ensures that $\boldsymbol{\pi}_\theta(t, X) \in \Delta^n$, meaning each component is nonnegative and sums to 1.

These networks are trained for 100,000 gradient steps using the Adam optimizer with a mini-batch size of 1,000. For problems involving up to $n = 10,000$ assets, a learning rate of 10^{-5} is typically used. However, when $n = 10,000$, this learning rate can sometimes cause instabilities during training, so it is reduced to 10^{-6} . In each iteration, the current policy is used to simulate forward, compute the resulting payoff, and perform backpropagation-through-time (BPTT) to update the parameters ϕ and θ . To prevent overfitting to any single dataset and to ensure broad coverage of the time-wealth domain $[0, T] \times [0.1, 2]$, the initial states (t_0, X_0) are dynamically redrawn in each mini-batch.

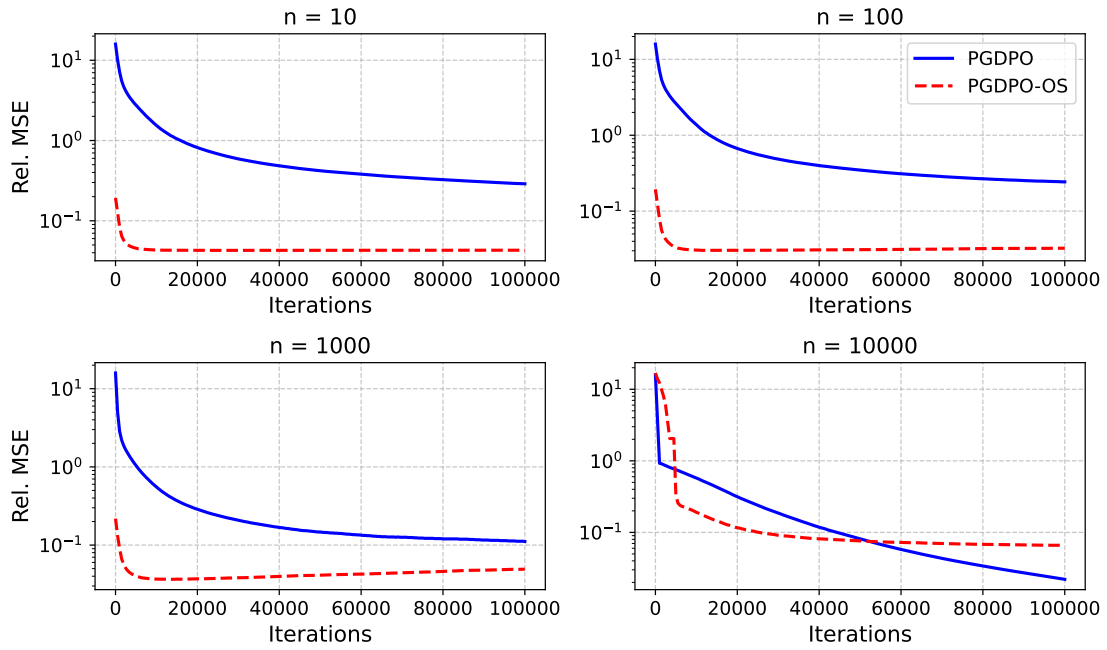
5.2 Unconstrained Multi-Asset Case

In this section, we test PG-DPO and its one-shot variant (PG-DPO-OneShot) on a multi-asset Merton problem without borrowing or short-sale constraints. Recalling Section 2.3, the unconstrained Merton model admits a closed-form solution for both the *investment* strategy $\boldsymbol{\pi}_t$ and the *consumption* rate C_t . This allows us to directly compare the learned neural policies with the true optimum in dimensions $n \in \{10, 100, 1000, 10000\}$.

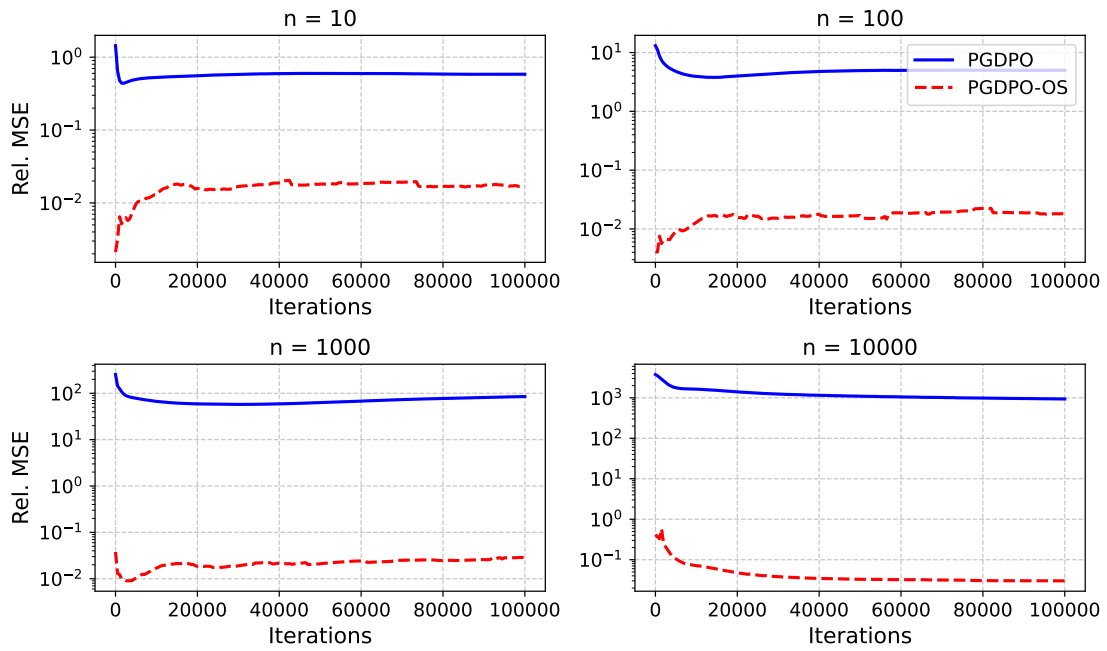
Table 2 provides a quantitative summary of the final (relative MSE) values for both *consumption* and *investment* under PG-DPO and PG-DPO-OneShot, evaluated at three iteration milestones (1,000, 10,000, and 100,000) across various asset dimensions $\{10, 100, 1000, 10000\}$. In higher dimensions, PG-DPO exhibits large residual errors, whereas PG-DPO-OneShot substantially reduces the MSE in both consumption and investment policies, demonstrating the scalability of Pontryagin-based direct policy optimization even for portfolios with thousands of assets.

Figures 1a and 1b illustrate how these methods converge by plotting mean-squared errors (MSE) relative to the closed-form benchmark. Figure 1a shows the *consumption* MSE, and Figure 1b shows the *investment* MSE across training iterations. One can see that PG-DPO consistently lags behind PG-DPO-OneShot in reducing error for both controls, especially in higher dimensions.

In particular, as shown in Figures 1a and 1b, the MSE for PG-DPO remains relatively high for both consumption (often above 10^{-1} or 10^{-2} well into training) and investment, whereas PG-DPO-OneShot typically achieves errors on the order of 10^{-3} (or lower) after just a few thousand iterations. This faster convergence arises from directly enforcing Pontryagin’s first-order conditions—for example, $(e^{-\rho t} U'(C_t^*) = \lambda_t)$ in the consumption case—rather than relying solely on the network output. A similar effect holds for the investment decision, where extracting the one-shot control from the adjoint process ensures more consistent



(a) Consumption MSE.



(b) Investment MSE.

Figure 1: Relative MSE results over 100k iterations. Panel (a) shows the *investment* policy MSE, while panel (b) shows the *consumption* policy MSE.

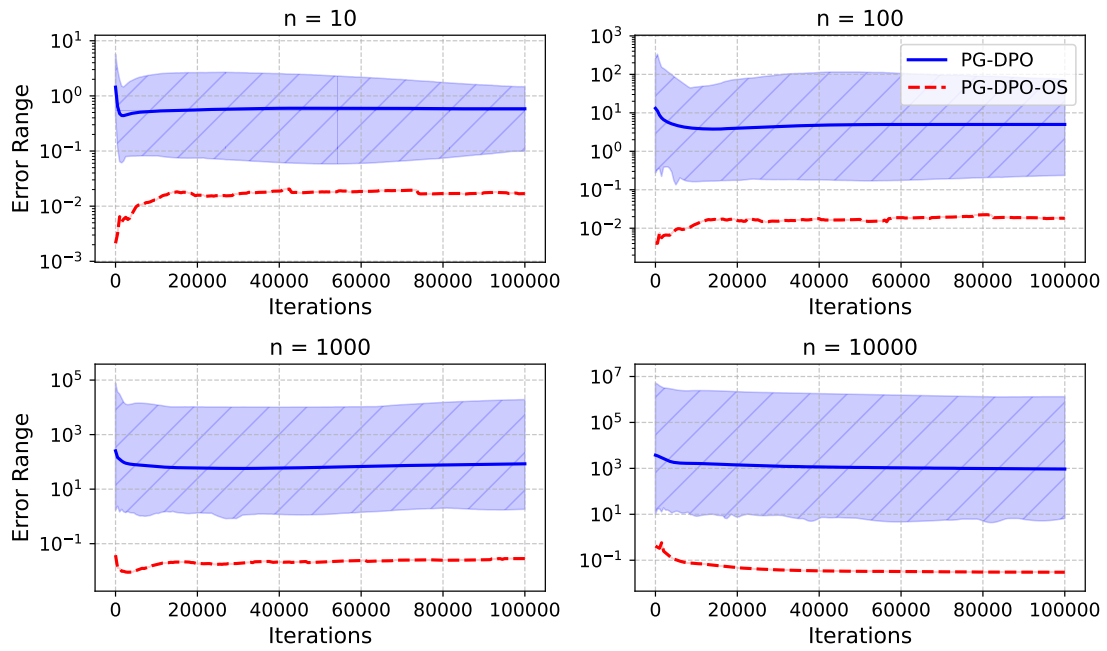


Figure 2: Min-max ranges of *investment* MSE across assets at each iteration.

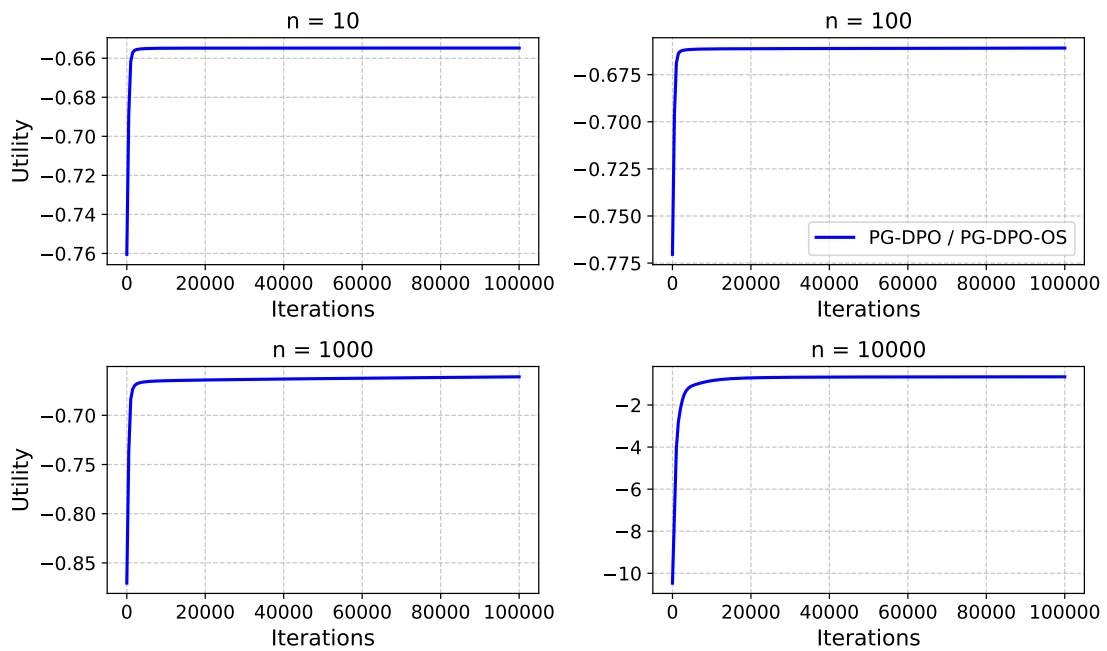


Figure 3: Empirical utility evolution (rolling 500-iteration averages).

Table 1: Relative MSE (lower is better) for consumption and investment under PG-DPO and PG-DPO-OneShot. Errors are recorded at iteration milestones {1k, 10k, 100k} for various dimensions $n = \{10, 100, 1000, 10000\}$.

Assets	Method	Consumption (MSE)			Investment (MSE)		
		1k	10k	100k	1k	10k	100k
10	PG-DPO	7.15e+00	1.54e+00	2.89e-01	4.77e-01	5.30e-01	5.84e-01
	PG-DPO-OS	8.40e-02	4.32e-02	4.30e-02	6.46e-03	1.29e-02	1.69e-02
100	PG-DPO	7.09e+00	1.37e+00	2.43e-01	8.70e+00	3.93e+00	4.99e+00
	PG-DPO-OS	7.84e-02	3.06e-02	3.24e-02	7.53e-03	1.29e-02	1.81e-02
1000	PG-DPO	2.85e+00	5.53e-01	1.11e-01	1.25e+02	6.69e+01	8.49e+01
	PG-DPO-OS	9.05e-02	3.67e-02	4.92e-02	1.23e-02	1.70e-02	2.84e-02
10000	PG-DPO	9.24e-01	5.75e-01	2.21e-02	3.20e+03	1.64e+03	9.36e+02
	PG-DPO-OS	1.23e+01	1.91e-01	6.61e-02	3.29e-01	7.10e-02	3.00e-02

alignment with the analytical optimum across all assets.

Moreover, our implementation on an RTX 4090 GPU confirms that 100,000 training iterations typically complete in about an hour, while just a few thousand iterations (requiring only 1–2 minutes) are often sufficient for PG-DPO-OneShot to yield near-optimal consumption and investment strategies across thousands of assets. This gap in training efficiency becomes even more pronounced as n grows.

Figure 2 further highlights the per-asset accuracy. Standard PG-DPO exhibits a broad min–max range of investment MSE (some assets remain poorly learned), whereas the one-shot solution collapses the band toward zero, enforcing a uniform relative accuracy across assets by leveraging a single scalar adjoint λ_t . Meanwhile, Figure 3 shows that both methods improve the overall discounted utility J over time, though utility alone can be less sensitive to multi-asset allocation details.

In conclusion, under the unconstrained multi-asset Merton setup—where analytic solutions are available—PG-DPO-OneShot routinely outperforms the baseline PG-DPO in both accuracy and speed of convergence for *both consumption and investment*, even as the number of risky assets grows to the thousands. By directly deploying Pontryagin’s conditions, the one-shot approach enforces consistent controls across all assets, requires far fewer training iterations, and scales effectively with modern GPU hardware.

5.3 Constrained Multi-Asset Case

We now consider a multi-asset Merton problem with *no short-selling or borrowing* constraints; i.e., each weight $\pi_{i,t}$ must lie in $[0, 1]$ and the total investment in risky plus risk-free assets sums to 1 at all times. Unlike the unconstrained setting of Section 5.2, no closed-form solution exists here. Consequently, we evaluate accuracy by measuring the *FOC residuals* (i.e., the deviation from Pontryagin’s

Table 2: MSEs of FOC residuals (lower is better) for consumption and investment under PG-DPO and PG-DPO-OneShot. Residuals are recorded at iteration milestones {1k, 10k, 100k} for various dimensions $n = \{10, 100, 1000\}$.

Assets	Method	Consumption (FOC Res.)			Investment (FOC Res.)		
		1k	10k	100k	1k	10k	100k
10	PG-DPO	4.89e+01	3.13e+04	1.46e+04	1.56e-02	3.42e-03	3.87e-01
	PG-DPO-OS	6.90e+03	2.64e+03	2.17e+03	1.25e-02	1.39e-04	1.90e-02
100	PG-DPO	4.82e+01	3.46e+02	3.13e+04	6.66e-04	8.58e-04	3.42e-03
	PG-DPO-OS	5.07e+03	3.01e+03	2.64e+03	9.33e-05	1.35e-04	1.39e-04
1000	PG-DPO	4.80e+01	3.84e+02	4.24e+04	1.93e-05	2.54e-05	2.53e-05
	PG-DPO-OS	8.03e+03	1.73e+03	3.19e+03	1.06e-06	1.51e-06	1.54e-06

first-order optimality conditions) for both π_t and C_t .

We only consider dimensions $n \in \{10, 100, 1000\}$. Although our method can train policies for $n = 10,000$ or more, computing the FOC-based residual metric in that regime is prohibitively expensive. In principle, a single barrier-based Newton solve for the OneShot control is fast enough, but *training the surrogate network* (see below) to describe the controls requires *many* repeated Newton solves at different (t, X) points. As n grows, these repeated solves dominate the computational cost, making it infeasible to measure and report FOC residuals at $n = 10,000$. Moreover, our implementation on an RTX 4090 GPU confirms that performing 10k training iterations (typically taking about 10 minutes) already yields stable performance, while running 100k iterations (about 1 hour) can achieve more robust and superior performance. Consequently, Table 2 presents *mean-square errors (MSE)* of the FOC residuals only for $n \leq 1000$ at the 1k, 10k, and 100k iteration marks, omitting the case $n = 10,000$ to avoid the excessive overhead required for repeatedly computing FOC residuals at high dimensions.

To estimate these residuals for the one-shot method, we train additional “surrogate” neural networks that replicates the policies implied by Pontryagin OneShot at each (t, X) . Specifically, during training, we simulate forward under the neural policy (π_t, C_t) to obtain costate samples λ_t and $\partial_x \lambda_t$, compute the barrier-based OneShot controls $(\pi_t^{\text{OS}}, C_t^{\text{OS}})$ for each step, and then use supervised learning to fit separate policy networks mapping $(t, X) \mapsto (\pi_t^{\text{OS}}, C_t^{\text{OS}})$. These new policy networks then allow us to simulate entire rollouts using OneShot-implied controls and measure the resulting FOC violations. As shown in Table 2, although PG-DPO-OneShot and PG-DPO may perform similarly in early iterations, the advantage of OneShot becomes much more pronounced over time. While PG-DPO often remains unstable or plateaus at a higher level of residual error, PG-DPO-OneShot continues to refine the costates and controls, ultimately yielding significantly lower consumption and investment residuals in alignment with Pontryagin’s conditions.

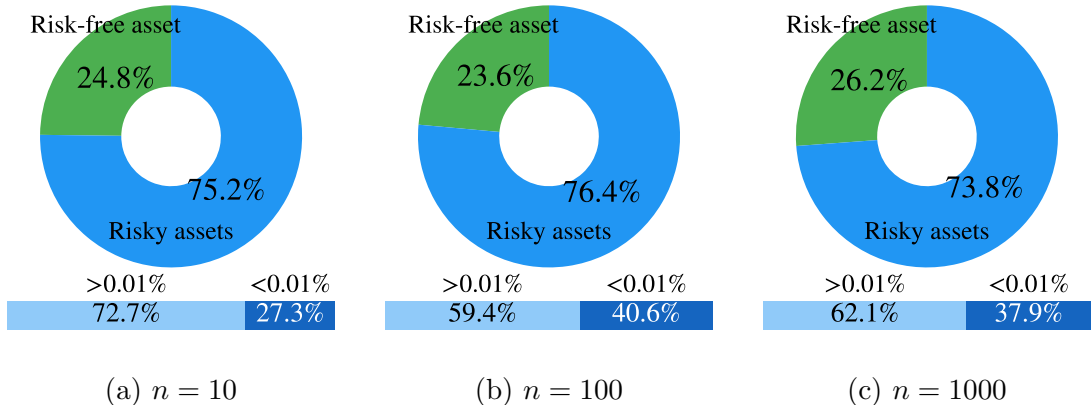


Figure 4: Donut charts of the *final learned portfolios* for different numbers of assets (n), illustrating the proportion of wealth allocated to the risk-free asset vs. risky assets. A separate bar plot (optional) indicates how many risky assets are assigned near-zero weights ($< 0.0001\%$) vs. those with larger allocations.

Figure 4 displays donut charts of the final learned portfolios for $n \in \{10, 100, 1000\}$. Across all dimensions, the model allocates roughly 25% of total wealth to the risk-free asset and 75% to risky assets. A noticeable fraction of risky assets—around 30% to 40%—receive less than 0.0001% of the total wealth, indicating that the model effectively *screens out* many assets by assigning them near-zero weights. The remaining risky assets share the bulk of the 75% portion.

In practice, empirical studies often find *even higher* proportions of assets pinned at or near zero, especially under no borrowing or short-selling constraints. This reflects the fact that, in real-world markets, a relatively small subset of risky assets can dominate performance while the vast majority contribute little. By contrast, in our synthetic setup, the drift and volatility parameters are designed so that allocations are somewhat more evenly distributed among risky assets. Hence, one should be mindful that certain calibration choices or real data could push a larger share of assets toward zero allocation.

In Figures 5–6, we visualize $\pi_i(t, X)$ for two representative assets under PG-DPO and PG-DPO-OneShot, respectively, after 10k training iterations. Each plot is a heatmap over the (t, X) domain, where the horizontal axis indicates current wealth X , the vertical axis indicates time t , and the color scale represents the magnitude of π_i .

In Figure 5, the chosen asset is one that receives a substantial fraction of total wealth under the optimal policy. PG-DPO exhibits a *curved* gradient from low to high values, suggesting that the network policy adjusts π_i in a more complex manner as t and X vary. By contrast, PG-DPO-OneShot yields a nearly *linear*

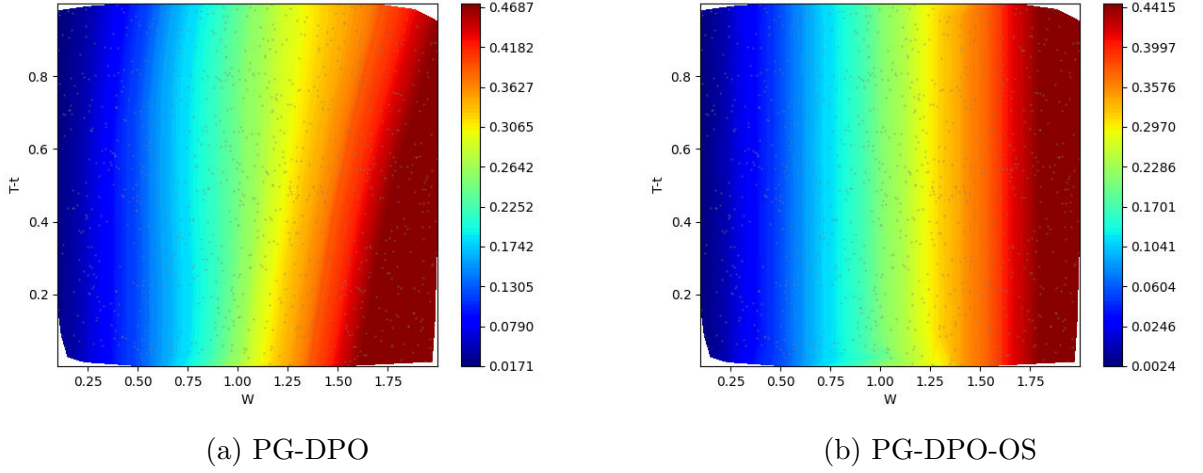


Figure 5: Learned policy $\pi_i(t, X)$ for an asset receiving a *nontrivial* share of wealth after 10k training iterations ($n = 10$). The PG-DPO solution (left) exhibits a somewhat curved profile over (t, X) , whereas the PG-DPO-OneShot solution (right) is nearly linear, consistent with CRRA intuition.

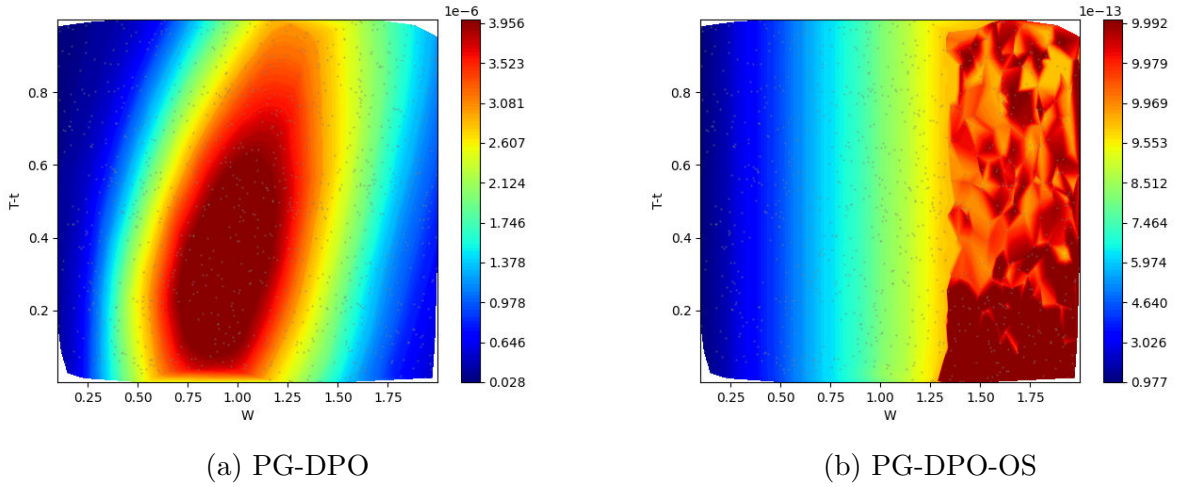


Figure 6: Learned policy $\pi_i(t, X)$ for an asset with *near-zero* optimal allocation after 10k training iterations ($n = 10$). While PG-DPO (left) still assigns small positive weights in some regions, PG-DPO-OneShot (right) more decisively pushes π_i close to zero, aligning better with the local Pontryagin optimum.

transition across the domain, which is consistent with CRRA-based intuition for smooth policy dependence on wealth and time.

A similar pattern emerges in Figure 6, where the optimal policy is nearly zero. Under PG-DPO, the color map shows small but nonzero patches, meaning the policy allocates a slight positive weight in certain (t, X) regions. Meanwhile, PG-DPO-OneShot pushes these allocations much closer to zero, aligning more closely with the local Pontryagin optimum. Overall, these examples reveal that while PG-DPO can capture broad utility improvements, it sometimes over- or under-allocates specific assets. In contrast, PG-DPO-OneShot, by enforcing first-order conditions at each point, achieves a cleaner partition between assets that merit investment and those that remain near-zero, producing a more interpretable and theoretically consistent policy shape across the (t, X) plane.

Overall, these results confirm that *OneShot* consistently enforces the barrier conditions more stringently than a purely network-based policy in high dimensions. Although PG-DPO is capable of improving utility and learning a feasible solution, its allocations often deviate from the local FOC conditions. By contrast, PG-DPO-OneShot uses the adjoint information to refine controls on each rollout, producing allocations that *both* maximize utility and better satisfy the Pontryagin-KKT conditions. While we do not report residuals for $n = 10,000$ (due to computational overhead in evaluating them), the same training workflow applies, and the policy remains fully scalable to large asset universes.

6 Conclusion

We have presented a Pontryagin-Guided Direct Policy Optimization (PG-DPO) framework that solves *large-scale* multi-asset Merton problems without relying on intractable dynamic programming grids. By weaving Pontryagin’s Maximum Principle (PMP) into a continuous-time neural-network parameterization, the method ensures that each gradient update follows locally optimal controls in expectation. Our experiments demonstrate that PG-DPO scales to portfolios with up to 10,000 risky assets, substantially extending earlier works that handled far fewer assets. Notably, in practice, even 100,000 gradient steps (enough to achieve very high accuracy) often complete in under an hour on a modern GPU, and around 10 minutes of training can already yield near-optimal solutions at virtually any dimension.

We have examined both the *unconstrained* and *constrained* (no short-selling or borrowing) cases. In the unconstrained setting, we verified that PG-DPO recovers the classical Merton solution across thousands of assets, achieving near-perfect alignment with the known closed-form formula. For the constrained setup, where no closed-form solution is available, we utilized barrier-based approaches to enforce portfolio feasibility (nonnegative weights summing to one) and optional consumption bounds. Even in this more realistic scenario, Pontryagin-based training converged reliably in high dimensions, overcoming the computational bottle-

necks associated with dynamic programming. Numerical results confirm that our method satisfies the Hamiltonian first-order conditions at each time step, thereby respecting the constraints while maximizing overall utility.

A particular advantage of the approach is the *PG-DPO-OneShot* variant, which uses a short warm-up training phase to stabilize the adjoint (costate) processes, and then computes near-optimal Pontryagin controls *directly*—through either a closed-form expression (unconstrained) or a fast barrier-based Newton solve (constrained)—at each time–state. This greatly reduces the need for prolonged network training and often achieves lower policy errors or first-order-condition (FOC) residuals, especially in higher dimensions. The one-shot procedure naturally accommodates portfolio constraints: it simply solves a low-dimensional barrier-augmented system at each time step, enforcing nonnegative weights that sum to unity. As a result, PG-DPO-OneShot yields accurate solutions and feasible controls, even with thousands of risky assets.

Our methodology opens several promising avenues for future work. First, while we have demonstrated large-scale capability under time-invariant drift and volatility, one can naturally extend the framework to time-varying parameters or more intricate dynamics (e.g., stochastic volatility, factor models, or regime switching). Second, many real-world constraints beyond short-sale or borrowing bans—such as transaction costs, consumption ratcheting, or regulatory/tax rules—can be incorporated into the Pontryagin-based approach by adjusting the state equations and constraint terms, though this may require more sophisticated numerical schemes. Third, robust or distributionally robust versions of dynamic portfolio choice can be studied by modifying the forward SDE or the costate equations accordingly. Finally, beyond power utility, one can consider other preference structures (e.g., habit formation, mean–variance, or prospect theory), so long as the first-order Pontryagin conditions are well-defined.

Overall, combining Pontryagin’s principle with modern deep backpropagation provides a robust, scalable solver for continuous-time, constrained dynamic portfolio optimization. It circumvents the curse of dimensionality that bedevils traditional dynamic programming or PDE approaches. By demonstrating feasibility for up to 10,000 (and potentially more) risky assets and achieving near-optimal performance within mere minutes of training, the hope is that this approach will further advance realistic, data-driven portfolio models and better capture the complexities of global financial markets.

Acknowledgments

This work was supported by the National Research Foundation of Korea (NRF) grant funded by the Korea government (MSIT) (RS-2024-00355646 and NRF-

2022R1F1A1063371).

References

- Balduzzi, P. & Lynch, A. W. (1999). Transaction costs and predictability: Some utility cost calculations. *Journal of Financial Economics*, 52(1), 47–78. 1
- Borkar, V. S. & Borkar, V. S. (2008). *Stochastic approximation: a dynamical systems viewpoint*, volume 9. Springer. 4.1
- Boyd, S. (2004). Convex optimization. *Cambridge UP*. 3.2.2
- Brandt, M. W., Goyal, A., Santa-Clara, P., & Stroud, J. R. (2005). A simulation approach to dynamic portfolio choice with an application to learning about return predictability. *The Review of Financial Studies*, 18(3), 831–873. 1
- Buraschi, A., Porchia, P., & Trojani, F. (2010). Correlation risk and optimal portfolio choice. *The Journal of Finance*, 65(1), 393–420. 1
- Campbell, J. Y., Chan, Y. L., & Viceira, L. M. (2003). A multivariate model of strategic asset allocation. *Journal of financial economics*, 67(1), 41–80. 1
- Campbell, J. Y. & Viceira, L. M. (1999). Consumption and portfolio decisions when expected returns are time varying. *The Quarterly Journal of Economics*, 114(2), 433–495. 1
- Campbell, J. Y. & Viceira, L. M. (2001). Who should buy long-term bonds? *American Economic Review*, 91(1), 99–127. 1
- Constantinides, G. M. (1990). Habit formation: A resolution of the equity premium puzzle. *Journal of political Economy*, 98(3), 519–543. 1
- Cvitanović, J. & Karatzas, I. (1996). Hedging and portfolio optimization under transaction costs: A martingale approach 1 2. *Mathematical finance*, 6(2), 133–165. 1
- Dai, M., Dong, Y., Jia, Y., & Zhou, X. Y. (2023). Learning merton’s strategies in an incomplete market: Recursive entropy regularization and biased gaussian exploration. *arXiv preprint arXiv:2312.11797*. 1, 5
- Dybvig, P. H. (1995). Dusenberry’s ratcheting of consumption: optimal dynamic consumption and investment given intolerance for any decline in standard of living. *The Review of Economic Studies*, 62(2), 287–313. 1

- Fiacco, A. V. & McCormick, G. P. (1990). *Nonlinear programming: sequential unconstrained minimization techniques*. SIAM. 3.2.2
- Fleming, W. H. & Soner, H. M. (2006). *Controlled Markov processes and viscosity solutions*, volume 25. Springer Science & Business Media. 1, 3.1
- Garlappi, L. & Skoulakis, G. (2010). Solving consumption and portfolio choice problems: The state variable decomposition method. *The Review of Financial Studies*, 23(9), 3346–3400. 1
- Han, J., Jentzen, A., & E, W. (2018). Solving high-dimensional partial differential equations using deep learning. *Proceedings of the National Academy of Sciences*, 115(34), 8505–8510. 1, 5
- Huh, J. (2024). A pontryagin-guided neural policy optimization framework for merton’s portfolio problem. *arXiv preprint arXiv:2412.13101*. 4, 4.4.2
- Jurek, J. W. & Viceira, L. M. (2011). Optimal value and growth tilts in long-horizon portfolios. *Review of Finance*, 15(1), 29–74. 1
- Karatzas, I., Lehoczky, J. P., & Shreve, S. E. (1987). Optimal portfolio and consumption decisions for a ”small investor” on a finite horizon. *SIAM journal on control and optimization*, 25(6), 1557–1586. 1
- Karatzas, I. & Shreve, S. E. (1998). *Methods of Mathematical Finance*. New York: Springer. 1
- Karush, W. (1939). Minima of functions of several variables with inequalities as side constraints. *M. Sc. Dissertation. Dept. of Mathematics, Univ. of Chicago*. 3.2.1, 3.2.1
- Kim, T. S. & Omberg, E. (1996). Dynamic nonmyopic portfolio behavior. *The Review of Financial Studies*, 9(1), 141–161. 1
- Kuhn, H. W. & Tucker, A. W. (2013). Nonlinear programming. In *Traces and emergence of nonlinear programming* (pp. 247–258). Springer. 3.2.1, 3.2.1
- Kushner, H. J. & Yin, G. G. (2003). *Stochastic Approximation and Recursive Algorithms and Applications*. New York: Springer Science & Business Media. 4.1
- Liu, J. (2007). Portfolio selection in stochastic environments. *The Review of Financial Studies*, 20(1), 1–39. 1

- Lynch, A. W. (2001). Portfolio choice and equity characteristics: Characterizing the hedging demands induced by return predictability. *Journal of Financial Economics*, 62(1), 67–130. 1
- Lynch, A. W. & Balduzzi, P. (2000). Predictability and transaction costs: The impact on rebalancing rules and behavior. *The Journal of Finance*, 55(5), 2285–2309. 1
- Ma, J. & Yong, J. (1999). *Forward-backward stochastic differential equations and their applications*. Number 1702. Springer Science & Business Media. 3.3
- Merton, R. C. (1969). Lifetime portfolio selection under uncertainty: The continuous-time case. *The review of Economics and Statistics*, (pp. 247–257). 1
- Merton, R. C. (1971). Optimum consumption and portfolio rules in a continuous-time model. *Journal of Economic Theory*, 3(4), 373–413. 1, 2
- Nocedal, J. & Wright, S. J. (1999). *Numerical optimization*. Springer. 3.2.1, 3.2.1, 3.2.2, 3.2.2
- Pardoux, E. & Peng, S. (1990). Adapted solution of a backward stochastic differential equation. *Systems & control letters*, 14(1), 55–61. 3.1
- Pham, H. (2009). *Continuous-time stochastic control and optimization with financial applications*, volume 61. Springer Science & Business Media. 3.1
- Pontryagin, L. S. (2018). *Mathematical theory of optimal processes*. Routledge. 3.1
- Raissi, M., Perdikaris, P., & Karniadakis, G. E. (2019). Physics-informed neural networks: A deep learning framework for solving forward and inverse problems involving nonlinear partial differential equations. *Journal of Computational physics*, 378, 686–707. 1, 5
- Reppen, A. M. & Soner, H. M. (2023). Deep empirical risk minimization in finance: Looking into the future. *Mathematical Finance*, 33(1), 116–145. 5
- Reppen, A. M., Soner, H. M., & Tissot-Daguette, V. (2023). Deep stochastic optimization in finance. *Digital Finance*, 5(1), 91–111. 5
- Samuelson, P. A. (1975). Lifetime portfolio selection by dynamic stochastic programming. *Stochastic optimization models in finance*, (pp. 517–524). 1
- Shreve, S. E. & Soner, H. M. (1994). Optimal investment and consumption with transaction costs. *The Annals of Applied Probability*, (pp. 609–692). 1

- Sundaresan, S. M. (1989). Intertemporally dependent preferences and the volatility of consumption and wealth. *Review of financial Studies*, 2(1), 73–89. 1
- Weinan, E. (2017). A proposal on machine learning via dynamical systems. *Communications in Mathematics and Statistics*, 1(5), 1–11. 1, 5
- Yong, J. & Zhou, X. Y. (2012). *Stochastic controls: Hamiltonian systems and HJB equations*, volume 43. Springer Science & Business Media. 3.3